Article

Immunity

Retinoic acid and TGF-β orchestrate organ-specific programs of tissue residency

Graphical abstract

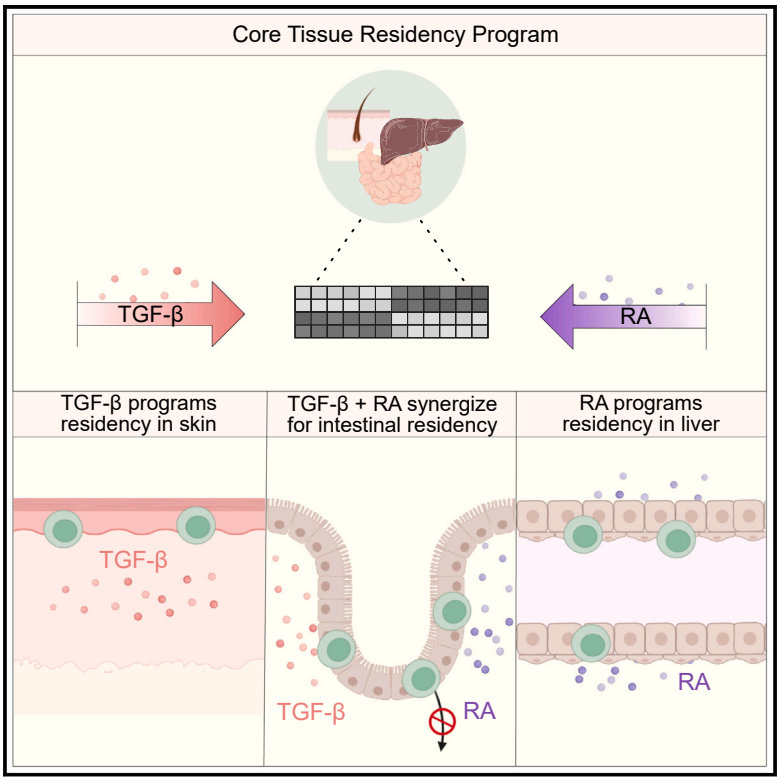

Authors

Andreas Obers, Tobias Poch, Grace Rodrigues, ..., Colby Zaph, Maximilien Evrard, Laura K. Mackay

Correspondence

maximilien.evrard@unimelb.edu.au (M.E.), lkmackay@unimelb.edu.au (L.K.M.)

In brief

CD8$^+$ T cells integrate signals from the local microenvironment to establish tissue residency, but which factors are involved and how remain unresolved. Obers et al. highlight the role of retinoic acid (RA) in promoting T_{RM} cell formation across multiple tissues and supporting intestinal T_{RM} cell maintenance by restricting their migration to draining lymph nodes.

Highlights

- CD8$^+$ T cells engage a RA-RARα-centered axis for tissue residency in multiple organs
- RA and TGF-β signals synergize to establish intestinal CD8$^+$ T cell immunity
- RA mediates intestinal T_{RM} cell maintenance by limiting their retrograde migration
- RA signaling replicates features of T_{RM} cells driven by microbial exposure

Obers et al., 2024, Immunity *57*, 2615–2633
November 12, 2024
https://doi.org/10.1016/j.immuni.2024.09.015

CellPress

Immunity

CellPress

Article

Retinoic acid and TGF-β orchestrate organ-specific programs of tissue residency

Andreas Obers,[1] Tobias Poch,[1] Grace Rodrigues,[2] Susan N. Christo,[1] Luke C. Gandolfo,[1,3,4] Raissa Fonseca,[1] Ali Zaid,[1] Joey En Yu Kuai,[1] Hongjin Lai,[1,5] Pirooz Zareie,[1] Marina H. Yakou,[6] Lachlan Dryburgh,[1] Thomas N. Burn,[1] James Dosser,[1] Frank A. Buquicchio,[7,8] Caleb A. Lareau,[7,8] Calum Walsh,[1] Louise Judd,[1] Maria Rafailia Theodorou,[9] Katharina Gutbrod,[10] Peter Dörmann,[10] Jenny Kingham,[11,12] Tim Stinear,[1] Axel Kallies,[1] Jan Schroeder,[1] Scott N. Mueller,[1] Simone L. Park,[1,13,14] Terence P. Speed,[3,4] Ansuman T. Satpathy,[7,8,15,16] Tri Giang Phan,[17,18] Christoph Wilhelm,[9] Colby Zaph,[2,19] Maximilien Evrard,[1,19,*] and Laura K. Mackay[1,19,20,*]

[1]Department of Microbiology and Immunology, The University of Melbourne at The Peter Doherty Institute for Infection and Immunity, Melbourne, VIC, Australia
[2]Biomedicine Discovery Institute, Department of Biochemistry and Molecular Biology, Monash University, Clayton, VIC, Australia
[3]School of Mathematics and Statistics, The University of Melbourne, Melbourne, VIC, Australia
[4]Walter and Eliza Hall Institute for Medical Research, Parkville, VIC, Australia
[5]Department of Thoracic Surgery and Institute of Thoracic Oncology, West China Hospital, Sichuan University, Chengdu, China
[6]Olivia Newton-John Cancer Research Institute, LaTrobe University School of Cancer Medicine, Heidelberg, VIC, Australia
[7]Department of Pathology, Stanford University, Stanford, CA, USA
[8]Program in Immunology, Stanford University, Stanford, CA, USA
[9]Immunopathology Unit, Institute of Clinical Chemistry and Clinical Pharmacology, University of Bonn, Bonn, Germany
[10]Institute for Molecular Physiology and Biotechnology of Plants, University of Bonn, Bonn, Germany
[11]Australian BioResources Pty Ltd, Moss Vale, NSW, Australia
[12]Animal Services, Garvan Institute of Medical Research, Darlinghurst, Sydney, NSW, Australia
[13]Institute for Immunology and Immune Health, Perelman School of Medicine, University of Pennsylvania, Philadelphia, PA, USA
[14]Department of Systems Pharmacology and Translational Therapeutics, Perelman School of Medicine, University of Pennsylvania, Philadelphia, PA, USA
[15]Parker Institute for Cancer Immunotherapy, Stanford University, Stanford, CA, USA
[16]Gladstone-UCSF Institute of Genomic Immunology, San Francisco, CA, USA
[17]Precision Immunology Program, Garvan Institute of Medical Research, Darlinghurst, Sydney, NSW, Australia
[18]St Vincent's Healthcare Clinical Campus, School of Clinical Medicine, Faculty of Medicine and Health, UNSW Sydney, Sydney, NSW, Australia
[19]Senior author
[20]Lead contact
*Correspondence: maximilien.evrard@unimelb.edu.au (M.E.), lkmackay@unimelb.edu.au (L.K.M.)
https://doi.org/10.1016/j.immuni.2024.09.015

SUMMARY

Tissue-resident memory T (T_{RM}) cells are integral to tissue immunity, persisting in diverse anatomical sites where they adhere to a common transcriptional framework. How these cells integrate distinct local cues to adopt the common T_{RM} cell fate remains poorly understood. Here, we show that whereas skin T_{RM} cells strictly require transforming growth factor β (TGF-β) for tissue residency, those in other locations utilize the metabolite retinoic acid (RA) to drive an alternative differentiation pathway, directing a TGF-β-independent tissue residency program in the liver and synergizing with TGF-β to drive T_{RM} cells in the small intestine. We found that RA was required for the long-term maintenance of intestinal T_{RM} populations, in part by impeding their retrograde migration. Moreover, enhanced RA signaling modulated T_{RM} cell phenotype and function, a phenomenon mirrored in mice with increased microbial diversity. Together, our findings reveal RA as a fundamental component of the host-environment interaction that directs immunosurveillance in tissues.

INTRODUCTION

The immune system safeguards tissue integrity by maintaining homeostasis and countering pathological and environmental challenges. Although immune cells residing in distinct organs possess unique qualities, they share the ability to survive long term in local niches, ensuring proper tissue function.[1–4] Among tissue-dwelling immune cells, tissue-resident memory T (T_{RM}) cells are specialized sentinels capable of controlling infections and malignancies, despite also being implicated in triggering

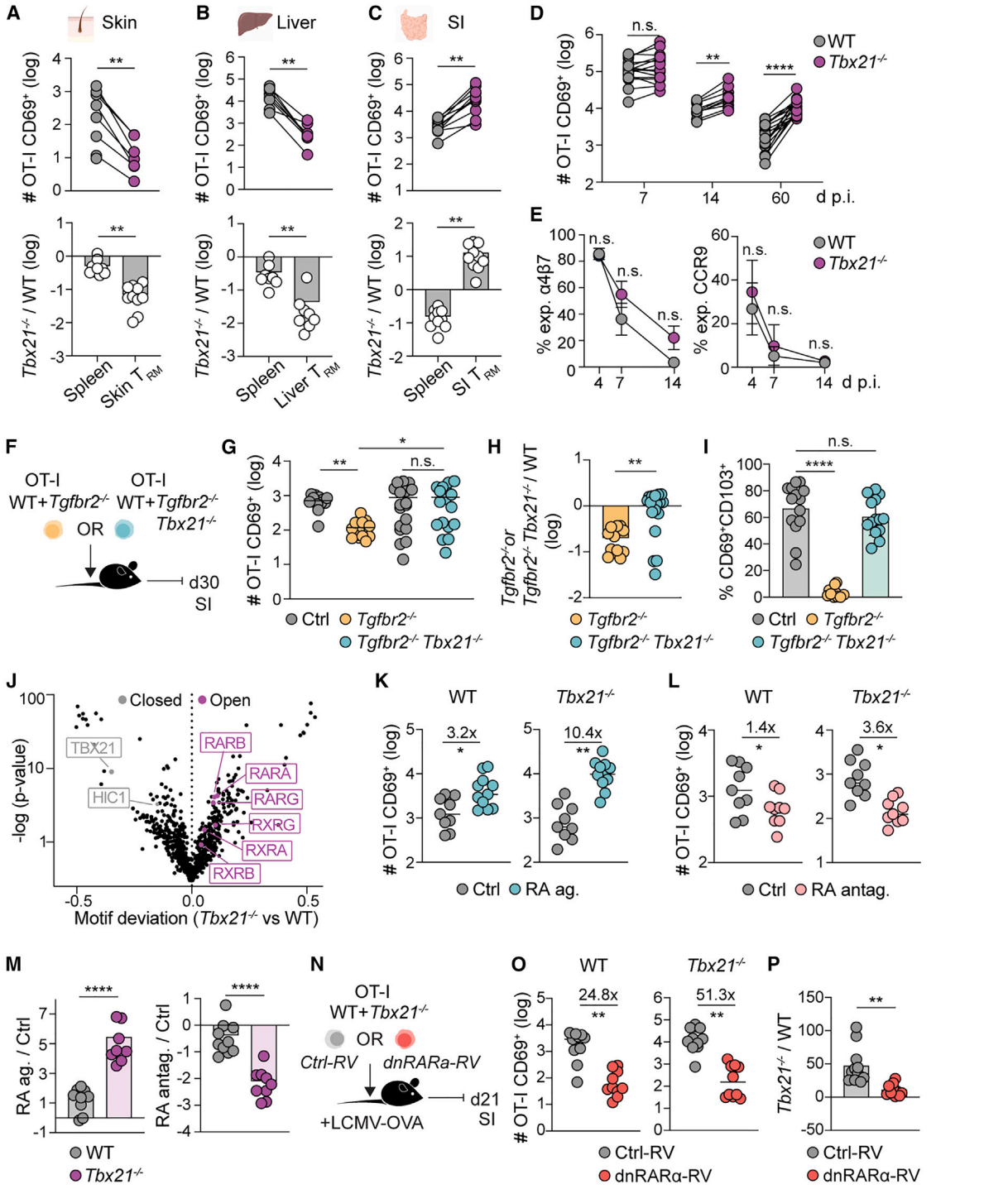

Figure 1. CD8⁺ T cells integrate RA signals as an alternative pathway for T_{RM} cell differentiation

(A–E) WT and *Tbx21*$^{-/-}$ OT-I cells were co-transferred into (A) HSV-OVA or (B–E) LCMV-OVA-infected mice. (A–C) OT-I cells were isolated >30 days post-infection (p.i.) from indicated tissues. (Top) Numbers of CD69⁺ OT-I cells from indicated tissues and (bottom) ratio of *Tbx21*$^{-/-}$ and WT OT-I cells. (D) Enumeration of SI CD69⁺ OT-I cells and (E) frequency of indicated molecules in mLN-derived OT-I cells at indicated times p.i.

(F–I) Effector WT and *Tgfbr2*$^{-/-}$ or *Tgfbr2*$^{-/-}$*Tbx21*$^{-/-}$ OT-I cells were co-transferred into recipient mice and isolated from the SI >30 days later as depicted in (F). (G) Enumeration and (H) ratio of CD69⁺ OT-I cells. (I) Frequency of CD69⁺CD103⁺ OT-I cells.

(J) WT and *Tbx21*$^{-/-}$ OT-I cells were primed with LCMV-OVA. SI CD69⁺ OT-I cells were sort-purified 8 days p.i. and subjected to ATAC-seq. Shown is the motif deviation derived from genes with differentially accessible chromatin regions between WT and *Tbx21*$^{-/-}$ OT-I cells.

(legend continued on next page)

autoimmune diseases.[5–8] Consequently, understanding how T_{RM} cell generation can be modulated is essential for developing targeted therapeutic interventions across multiple disease settings.

The tissue milieu is vital in guiding T_{RM} cell development. It shapes immune cell fate, phenotype, and function through cytokines and metabolites that anchor immune cells in their local cellular ecosystem.[9,10] Although tissue microenvironments are diverse in nature, they converge to produce molecules that enhance local retention and repress tissue egress pathways, establishing a common residency program in tissue-localizing lymphocytes.[11–13] Transforming growth factor-β (TGF-β) is a key conductor of the tissue residency program, particularly at epithelial barriers where it modulates transcriptional regulators such as Eomes and T-bet[14] and promotes expression of adhesive molecules, including CD103.[14–16] Additionally, TGF-β balances T_{RM} cell proliferation, maintenance, and functionality by regulating the expression of checkpoint inhibitory molecules, protecting tissues from excessive damage.[17]

T_{RM} cells in non-epithelial sites, such as the liver, exhibit core T_{RM} cell transcriptional characteristics regulated independently of TGF-β,[13,17] indicating that additional organ-specific features promote tissue residency. Beyond host-derived factors, commensal bacteria and their metabolites—including retinoic acid (RA), secondary bile acids, and short-chain fatty acids—also influence the orchestration of T cell responses.[18–20] The vitamin-A-derived metabolite RA is essential for maintaining immune tolerance by instructing $CD4^+$ T cell differentiation, promoting regulatory T cell (T_{reg}) induction while inhibiting the T helper (Th) 17 program.[21] Moreover, RA imparts tissue-homing properties on both $CD4^+$ and $CD8^+$ T cells by inducing α4β7 and CCR9 expression, guiding their migration to the small intestine (SI).[22] However, the role of RA in fostering tissue residency and the influence of this metabolite on immunity beyond the intestine remain enigmatic.

Here, we reveal the multifaceted role of RA in regulating tissue immunity. We find that RA is a pivotal factor in directing the tissue-resident transcriptional program in the liver and SI, where RA synergizes with TGF-β to drive T_{RM} cell development. SI T_{RM} cells conditioned by heightened RA signaling persisted independently of TGF-β, implying redundancy between these factors. Furthermore, RA signaling shapes the abundance, phenotype, function, and maintenance of T_{RM} cells, with RA signaling blockade facilitating their egress from the SI to draining lymph nodes (LNs). Altogether, this work highlights RA as a major coordinator of immunological memory in tissues, offering avenues to enhance local immunity in therapeutic settings.

RESULTS

$CD8^+$ T cells integrate RA signals as a distinct pathway for tissue residency

The transcription factor (TF) T-bet coordinates $CD8^+$ T cell differentiation, balancing effector and memory T cell generation[23] and driving T_{RM} cell development across various tissues.[14,17,24] Whereas skin and liver T_{RM} cells rely on T-bet and downstream interleukin (IL)-15 signals for survival (Figures 1A, 1B, and S1A), SI T_{RM} cells are maintained independently of IL-15,[25] suggesting a T-bet-independent development pathway. Indeed, in experiments using $CD8^+$ ovalbumin ($OVA_{257–264}$)-specific OT-I transgenic T cells sufficient (wild type [WT]) or deficient for T-bet (*Tbx21*$^{-/-}$) in combination with recombinant herpes simplex virus (HSV) or lymphocytic choriomeningitis virus (LCMV) expressing OVA infection models, we found that, unlike T_{RM} cells in the skin and liver, SI T_{RM} cells flourished in the absence of T-bet (Figures 1A–1C). This enhanced SI T_{RM} cell generation was not attributable to enhanced tissue entry during the acute phase of infection nor due to differential expression of the intestinal-homing molecules, α4β7 and CCR9 (Figures 1D and 1E). Rather, T-bet-deficient OT-I cells in SI demonstrated robust persistence over time, whereas WT cells gradually declined (Figure 1D).

Previous studies have highlighted the importance of CD103 in facilitating SI T_{RM} cell retention.[15,26] T-bet directly binds to the *Itgae* gene locus,[24] resulting in elevated CD103 expression in *Tbx21*$^{-/-}$ cells (Figure S1B). Accordingly, we hypothesized that increased CD103 expression might facilitate *Tbx21*$^{-/-}$ cell persistence. To test this, we ablated CD103 (*sgItgae*) in WT and *Tbx21*$^{-/-}$ OT-I cells via CRISPR-Cas9 (Figures S1C and S1D). Although CD103 deletion in WT cells led to reduced SI T_{RM} cells, *Tbx21*$^{-/-}$ cells were numerically unchanged (Figure S1E), indicating that increased *Tbx21*$^{-/-}$ cell lodgment is independent of CD103. Although CD103 plays a role in T_{RM} cell retention, it operates within a broader T_{RM} cell differentiation program orchestrated by the cytokine TGF-β.[17] To investigate whether *Tbx21*$^{-/-}$ cells may exhibit increased sensitivity to TGF-β, we co-transferred effector WT with *Tgfbr2*$^{-/-}$ or *Tgfbr2*$^{-/-}$*Tbx21*$^{-/-}$ OT-I cells into recipient mice and isolated SI T_{RM} cells > 30 days later (Figure 1F). In the absence of T-bet, SI T_{RM} cells circumvented their reliance on the canonical TGF-β pathway and, furthermore, displayed a prototypical SI T_{RM} cell phenotype, including CD103 expression, which is typically controlled by TGF-β (Figures 1G–1I).

This observation implied that T-bet-deficient $CD8^+$ T cells utilize alternative tissue cues to engage tissue residency. To investigate the molecular changes underpinning this distinction, we employed assay of transposase-accessible chromatin sequencing (ATAC-seq) to assess differential chromatin accessibility between WT and *Tbx21*$^{-/-}$ OT-I cells isolated from the SI post LCMV-OVA infection. Among 6,828 differentially accessible chromatin sites

(K–M) Effector WT and *Tbx21*$^{-/-}$ OT-I cells were co-transferred into naive recipients. Mice were treated every other day with DMSO (Ctrl), AM80 (RA agonist [ag.]), or AGN194310 (RA antagonist [antag.]) from 0 to 6 days post transfer and SI OT-I cells were isolated 30 days post transfer. (K and L) Enumeration and (M) ratios of WT and *Tbx21*$^{-/-}$ OT-I cells from RA-ag.- or RA-antag.-treated mice compared with Ctrl-treated mice.
(N–P) WT and *Tbx21*$^{-/-}$ OT-I cells were transduced with either empty (Ctrl-RV) or dnRARα (dnRARα-RV) retroviruses. Transduced OT-I cells were co-transferred into LCMV-OVA-infected mice and isolated from the SI 21 days p.i., as depicted in (N). (O) Enumeration and (P) ratio of WT and *Tbx21*$^{-/-}$ OT-I cells transduced with Ctrl-RV or dnRARα-RV. Data are pooled from 2 to 3 independent experiments (A, B, D, G–I, and K–P) or representative of 1–3 independent experiments (C, E, and J–L) with $n = 8–17$ (A, B, and D) or $n = 3–8$ (C, E, G–I, and K–P) mice per group. *$p \leq 0.05$, **$p \leq 0.01$, ****$p \leq 0.0001$, n.s., non-significant, Wilcoxon test (A, B, and E), paired t test (C, D, and G), unpaired t test (H, I, and K–P). Bars represent the mean; symbols represent individual mice.

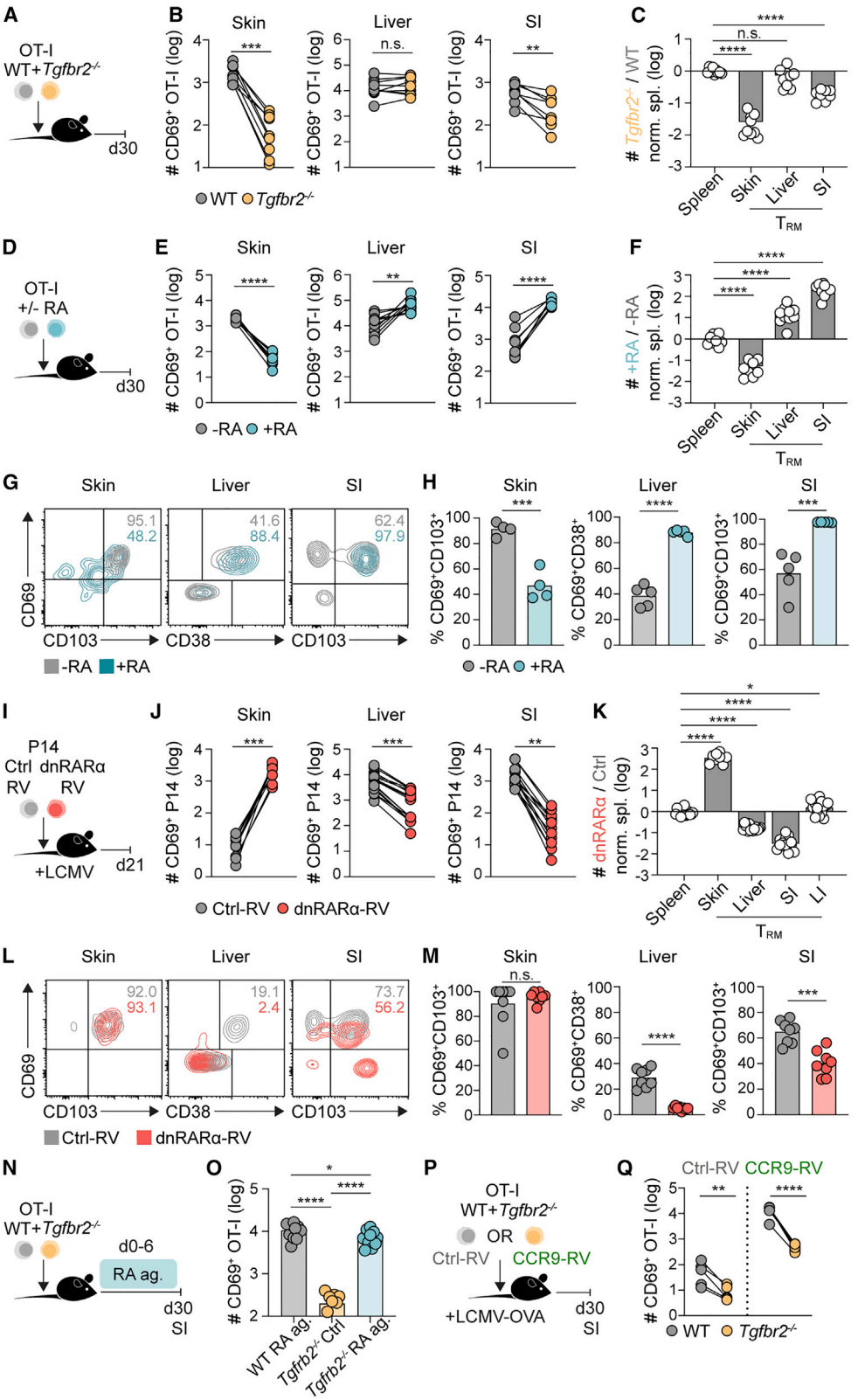

Figure 2. RA and TGF-β signals choreograph T_{RM} cell tropism across organs

(A–C) Effector WT and *Tgfbr2*$^{-/-}$ OT-I cells were co-transferred into DNFB-treated mice and isolated from indicated tissues 30 days later, as depicted in (A). (B) Enumeration and (C) ratio of *Tgfbr2*$^{-/-}$ and WT OT-I cells in indicated tissues.

(legend continued on next page)

identified, cells lacking T-bet exhibited increased accessibility for TF motifs associated with T_{RM} cell differentiation, such as *Bhlhe40*, *Prdm1*, and *Fos*,[13,27–29] and for T_{RM}-cell-associated genes such as *Itgae* and *Ccr9*[11,13] (Figures S1F and S1G). In contrast, T-bet-deficient cells showed decreased accessibility for TF motifs associated with T_{CIRC} cells such as *Eomes*[14] and for T_{CIRC}-cell-associated genes such as *S1pr1* and *Sell*[11,13] (Figures S1F and S1G). Pathway enrichment analyses revealed that *Tbx21*$^{-/-}$ cells displayed increased accessibility in genes involved in RA signaling compared with WT cells (Figure S1H), and exhibited greater accessibility in RA-related motifs, including nuclear receptors such as retinoic acid receptor (RAR) and retinoid X receptor (RXR) isoforms, as well as reduced motifs for Hic1 (Figure 1J), an RA-responsive transcriptional repressor that promotes SI T_{RM} cell differentiation.[30,31] Further, examination of RAR, RXR, and Hic1 gene loci revealed the largest change in peak accessibility in *Rara* and *Hic1* genes in *Tbx21*$^{-/-}$ cells (Figure S1I), with multiple T-bet-binding sites at *Rara* and *Hic1* loci (Figure S1J), indicating that T-bet may directly control these TFs. In line with this, we found that upon culture with RA *in vitro*, *Tbx21*$^{-/-}$ cells exhibited enhanced protein expression of RA-dependent molecules such as α4β7, CCR9, and Hic1 (Figures S1K and S1L), suggesting that T-bet limits RA responsiveness.

To investigate whether T_{RM} cell formation could be directly influenced by RA and T-bet interplay, we employed a RARα/β agonist (AM80; RA ag.) and pan-RA receptor antagonist (AGN194310; RA antag.) to modulate RA signaling *in vivo*. To this end, we transferred effector WT and *Tbx21*$^{-/-}$ OT-I cells into mice that were treated with either agent for 6 days or left untreated as a control (Ctrl). As anticipated, WT T_{RM} cells in the SI were numerically increased or decreased upon RA agonism or antagonism, respectively (Figures 1K and 1L). In addition, the effect of both agents was more pronounced in *Tbx21*$^{-/-}$ cells (Figures 1K–1M and S1M), suggesting that T-bet modulates RA responsiveness *in vivo*. To explore whether this effect was cell intrinsic, we employed WT and *Tbx21*$^{-/-}$ OT-I cells expressing a dominant-negative form of RARα (dnRARα),[32] which abrogates RA signaling (Figure S1N). Upon tracking WT and *Tbx21*$^{-/-}$ OT-I cells transduced with dnRARα or Ctrl retroviruses in LCMV-OVA-infected mice, we found that dnRARα expression prevented the enhanced persistence of T-bet-deficient SI T_{RM} cells (Figures 1N–1P). Conversely, the deletion of Hic1 in *Tbx21*$^{-/-}$ OT-I cells did not alter SI T_{RM} cell persistence compared with WT cells (Figures S1O–S1Q), suggesting that the heightened RA sensitivity observed in T-bet-deficient cells relies on RARα rather than Hic1. Thus, CD8$^+$ T_{RM} cell abundance in the SI is regulated by intersecting transcriptional and cytokine circuits, with T-bet expression controlling the integration of RA signals through RARα.

RA and TGF-β signaling differentially direct T_{RM} cell development across organs

Our results so far indicate that T_{RM} cells can persist in the SI in the absence of T-bet through sustained RA signaling, bypassing their archetypal reliance on TGF-β. Indeed, whereas T_{RM} cells at barrier sites, including the SI and skin, are strictly dependent on TGF-β for development,[14,16] those in non-epithelial organs such as the liver exist independently of this cytokine[17] (Figures 2A–2C). Hence, we reasoned that T_{RM} cells at distinct tissue locations might also exhibit unique dependencies on extrinsic RA, with RA substituting for TGF-β in sites where the latter is dispensable. To test this, we treated *in vitro*-activated OT-I cells with RA prior to transfer into naive mice treated with the contact sensitizer DNFB, to "pull" cells into the skin as described,[33] and enumerated T_{RM} cells > 30 days later. Although RA-treated cells showed impaired infiltration and T_{RM} cell differentiation in the skin, RA enhanced T_{RM} cell development in the SI and liver, with >85% of OT-I cells adopting a T_{RM} cell phenotype in these organs (Figures 2D–2H). This indicated that skin and liver T_{RM} cells depend on either TGF-β or RA, respectively, whereas SI T_{RM} cells engage both factors for development.

To explore the role of RA signaling in T_{RM} cell differentiation across organs, we transferred LCMV $GP_{33–41}$-specific P14 T cells transduced with dnRARα or Ctrl retroviruses into LCMV-infected mice. During the acute phase of infection (8 days post-infection [p.i.]), disruption of the RA-RARα axis prevented the formation of short-lived effector cells (KLRG1$^+$CD127$^-$), leading to increased numbers of memory precursor cells (KLRG1$^-$CD127$^+$) in lymphoid tissues (Figures S2A and S2B), consistent with previous observations.[34] Additionally, dnRARα CD69$^+$ T_{RM} cell precursors were reduced in the liver and SI (Figures S2C and S2D), indicating that although detrimental for the generation of circulating memory precursors, RA signaling is essential for T_{RM} cell differentiation. During the memory phase of infection (21 days p.i.), dnRARα T_{RM} cell numbers were reduced in the liver, kidney, and SI, increased in the skin, and remained unchanged in other tissues, including the large intestine (LI) (Figures 2I–2M

(D–H) Effector OT-I cells, with or without RA, transferred into DNFB-treated mice and isolated from indicated tissues 30 days later, as depicted in (D). (E) Enumeration and (F) ratio of ±RA-cultured OT-I cells in indicated tissues. (G) Expression of CD38, CD69, and CD103 in ±RA-cultured OT-I cells from indicated tissues, and (H) frequency of CD69$^+$CD103$^+$ (*skin*, *SI*) CD69$^+$CD38$^+$ (*liver*) OT-I cells isolated from indicated tissues and culture conditions.

(I–M) P14 cells were transduced with either empty (Ctrl-RV) or dnRARα (dnRARα-RV) retroviruses, co-transferred into LCMV-infected, DNFB-treated recipient mice and isolated from indicated tissues 21 days p.i., as depicted in (I). (J) Enumeration and (K) ratio of Ctrl-RV or dnRARα-RV P14 cells in indicated tissues. (L) Expression of indicated markers in Ctrl-RV or dnRARα-RV P14 cells from indicated tissues, and (M) frequency of CD69$^+$CD103$^+$ (*skin*, *SI*) CD69$^+$CD38$^+$ (*liver*) Ctrl-RV or dnRARα-RV P14 cells isolated from indicated tissues.

(N–Q) Effector WT and *Tgfbr2*$^{-/-}$ OT-I cells were co-transferred into naive recipients. Mice were treated with DMSO (Ctrl) or AM80 (RA ag.) from 0 to 6 days post transfer and SI OT-I cells were isolated 30 days post transfer, as depicted in (N). (O) Numbers of CD69$^+$ OT-I cells for indicated genotypes and treatments. (P and Q) Effector WT and *Tgfbr2*$^{-/-}$ OT-I cells were transduced with either empty (Ctrl-RV) or CCR9 (CCR9-RV) retroviruses, co-transferred into LCMV-OVA-infected recipients and isolated from the SI 30 days p.i., as depicted in (P). (Q) Numbers of transduced SI CD69$^+$ OT-I cells for indicated genotypes and experimental groups. Data are pooled from 2 to 3 independent experiments (A–F and J–Q) or representative of 2 independent experiments (H) with $n = 7–10$ or $n = 4–5$ (H) mice per group, $^*p \leq 0.05$ $^{**}p \leq 0.01$, $^{***}p \leq 0.001$, $^{****}p \leq 0.0001$, n.s., non-significant, paired t test (B, E, J, and Q), unpaired t test (H and M), ordinary one-way ANOVA with Tukey's multiple comparisons test (K), or ANOVA with Tukey's multiple comparisons test (C, F, and O). Bars represent the mean; symbols represent individual mice.

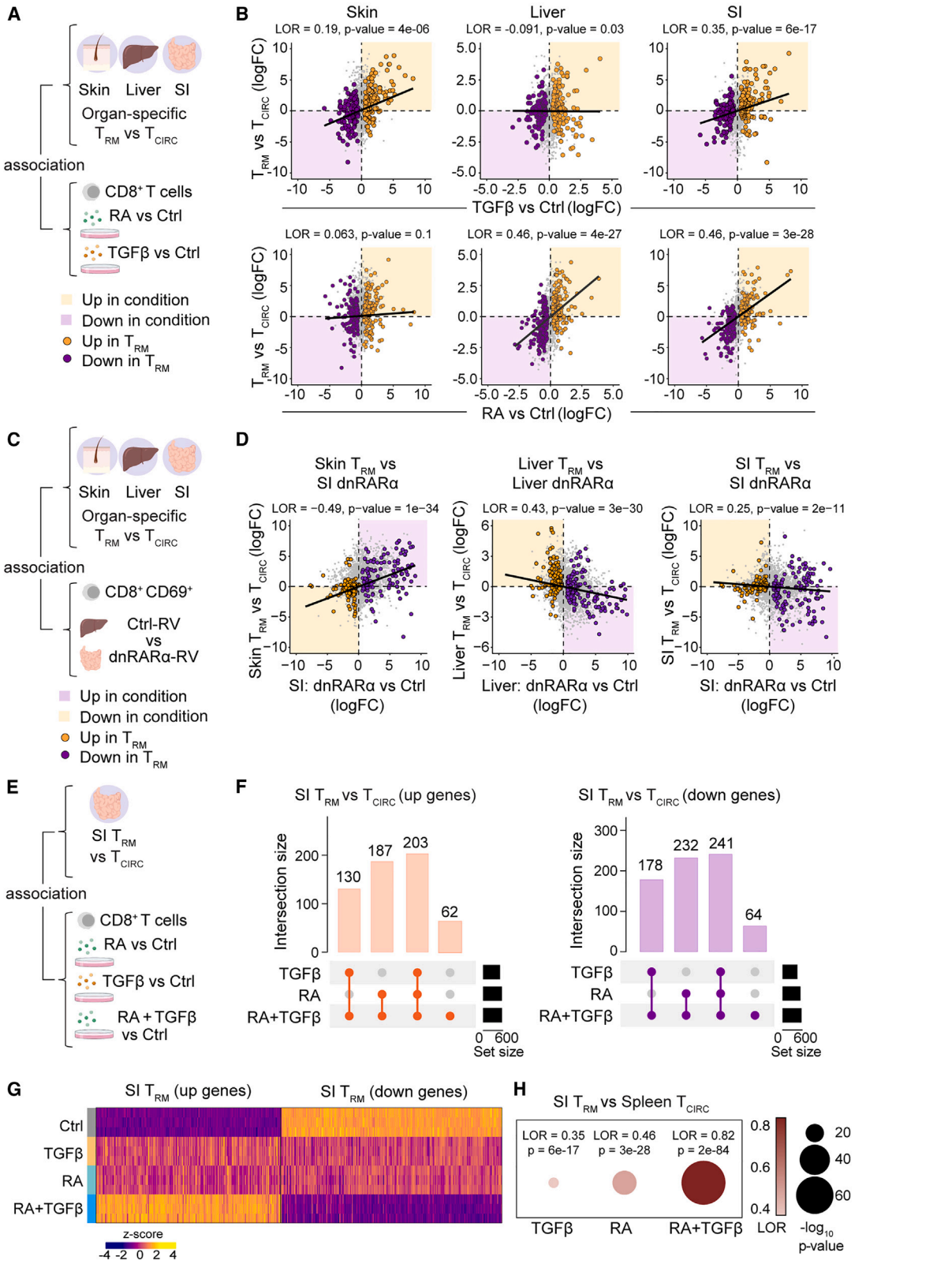

Figure 3. RA and TGF-β signals differentially program tissue residency across organs

(A–B) Effector CD8+ T cells were cultured in the absence (Ctrl) or presence of TGF-β, RA, or RA + TGF-β for 7 days, and subjected to RNA-seq. (A and B) Gene expression data from TGF-β- or RA-cultured CD8+ T cells was compared with skin, liver, and SI T_{RM} cell transcriptional signatures from GEO: GSE70813,[13] as

(legend continued on next page)

and S2E–S2G). In line with this, dnRARα cells also showed impaired T_{RM} cell formation in the liver and SI, but not LI in the context of enteric *Listeria monocytogenes* infection, revealing the compartmentalized requirement for RA in the intestine (Figures S2H–S2J). Furthermore, deletion of the RA-induced TF Hic1 in T cells impaired T_{RM} cell formation in the liver and SI but not in the skin (Figures S2K–S2M), suggesting overlapping roles for RARα and Hic1 in RA signaling in the liver and SI but distinct roles in the skin.

To investigate whether RA could compensate for a lack of TGF-β signaling in SI T_{RM} cells, we agonized RA signaling in *Tgfbr2*$^{-/-}$ OT-I cells. We found that RA agonism enhanced the number of *Tgfbr2*$^{-/-}$ OT-I cells in the SI (Figures 2N, 2O, and S2N), resonating with observations made in the context of T-bet deficiency (Figures 1G–1I). To determine whether the recovery of SI T_{RM} cells was solely due to increased migration of effector T cells from enhanced RA signaling, we forced CCR9 expression in WT and *Tgfbr2*$^{-/-}$ OT-I cells and assessed SI T_{RM} cell development over time (Figure 2P). Although CCR9 overexpression increased T cell entry into the SI (Figures S2O and S2P), it did not rescue the maintenance defect of *Tgfbr2*$^{-/-}$ OT-I T_{RM} cells (Figure 2Q). Thus, augmenting RA signaling allows SI T_{RM} cells to circumvent their canonical dependence on TGF-β.

RA and TGF-β modulate organ-specific gene signatures associated with T_{RM} cells

We have previously shown that TGF-β drives a plethora of gene changes associated with skin T_{RM} cell transcriptional programming.[17] However, given this cytokine is dispensable in liver T_{RM} cells that engage a similar tissue residency gene program, this raises questions as to how parallel tissue-resident features are induced in developmentally diverse T_{RM} cell populations. We therefore asked whether additional microenvironmental factors such as RA might replicate the action of TGF-β in driving T_{RM}-cell-associated transcriptional changes. To investigate tissue residency-associated gene alterations induced by RA or TGF-β signaling, we performed RNA sequencing (RNA-seq) on *in vitro*-activated CD8$^+$ T cells cultured in the presence or absence (Ctrl) of these factors. We then compared these gene expression changes to established transcriptional signatures of T_{RM} cells derived from either the skin, liver, or SI versus T_{CIRC} cells[13] (Figure 3A). Here, we found a positive association between the global gene expression in TGF-β-cultured cells and skin and SI T_{RM} cell organ-specific signatures but not the liver T_{RM} cell signature. In contrast, RA-cultured cells exhibited gene expression changes associated with SI and liver T_{RM} cells but not skin T_{RM} cells (Figure 3B). Numerous genes modulated by TGF-β that were enriched in skin and SI T_{RM} cells, and genes induced by RA that were enriched in SI and liver T_{RM} cells, were associated with microenvironmental interactions, including response to danger or stress (*P2rx7*, *Klrc1*, and *Klrk1*) as well as cytokine responsiveness (*Il6ra*, *Il27ra*, and *Evi5*) (Figure S3A). To determine whether RA-driven transcriptional changes occurred *in vivo*, we profiled the transcriptome of Ctrl and dnRARα CD69$^+$ T_{RM} cells in the liver and SI 14 days after LCMV infection (Figure 3C). Consistent with the defect in liver and SI T_{RM} cell differentiation observed in the absence of RA signaling, dnRARα cells showed gene expression changes associated with a loss of liver and SI T_{RM} cell signatures (Figure 3D). This correlation was accompanied by increased expression of T_{CIRC}-cell-associated genes related to tissue egress (*Ccr7*, *S1pr1*, *S1pr4*) and cell migration (Figures S3B and S3C). Additionally, the lack of RA signaling in SI T_{RM} cells caused gene expression changes characteristic of skin T_{RM} cells, including the expression of homing molecules (*Ccr8* and *Ccr10*) (Figures 3D and S3B), which aligns with the enhanced T_{RM} cell differentiation of dnRARα cells in this tissue (Figures 2I–2M). Together, these results show that although RA or TGF-β induce transcriptional changes associated with either liver or skin T_{RM} cells, respectively, both of these factors instruct the transcriptional signature of T_{RM} cells in the SI.

RA and TGF-β signaling synergize to shape intestine-specific T_{RM} cell identity

Our results indicate that both RA and TGF-β contribute to the differentiation of SI T_{RM} cells. Thus, we next asked whether the impact of these factors on T_{RM} cell programming is additive or whether their combined action drives a unique outcome. To explore this, we compared gene expression changes induced by RA, TGF-β, or RA + TGF-β in CD8$^+$ T cells to the gene signature of T_{RM} cells in the SI (Figure 3E). In line with our findings that increased RA signaling can compensate for the lack of TGF-β (Figures 2N and 2O), we observed substantial overlap among the different culture conditions, suggesting that the combined action of RA and TGF-β drives a similar set of genes within the SI T_{RM} cell gene signature (Figure 3F). However, upon evaluating SI-specific genes shared across culture conditions, the combination of RA and TGF-β resulted in a gene expression pattern more closely associated with the SI T_{RM} cell gene signature compared with their individual effects (Figure 3G). Moreover,

depicted in (A). (B) Scatterplots showing transcriptional changes for skin, liver, and SI T_{RM} cells vs. splenic T_{CIRC} cells (*y axis*) against CD8$^+$ T cells cultured with (top) TGF-β or (bottom) RA vs. Ctrl (*x axis*). Dots represent the top 200 genes with increased (orange) or decreased (purple) expression in T_{RM} cells from indicated tissues vs. T_{CIRC} cells. Black line represents least-squares regression line fitted to all points.

(C and D) P14 cells were transduced with either empty (Ctrl-RV) or dnRARα (dnRARα-RV) retroviruses and co-transferred into LCMV-infected recipient mice. Liver and SI CD69$^+$ transduced P14 cells were sort-purified 14 days p.i. and subjected to bulk RNA-seq. CD69$^+$ P14 cells gene expression data from indicated tissues and experimental groups was compared to skin, liver, and SI T_{RM} cell transcriptional signatures from GEO: GSE70813,[13] as depicted in (C). (D) Scatterplots showing transcriptional changes for skin, liver, and SI T_{RM} cells vs. splenic T_{CIRC} cells (*y axis*) against Ctrl-RV vs. dnRARα-RV CD69$^+$ P14 cells (*x axis*) from indicated tissues. Dots represent the top 200 genes with increased (orange) or decreased (purple) expression in T_{RM} cells from indicated tissues vs. T_{CIRC} cells. Black line represents least-squares regression line fitted to all points.

(E–H) SI T_{RM} cell transcriptional signature (GEO: GSE70813 [13]) was compared with gene expression data from TGF-β, RA, or RA + TGF-β-cultured CD8$^+$ T cells, as depicted in (E). (F) UpSet plots showing SI T_{RM} cell signature genes and their DE status within CD8$^+$ T cells cultured with TGF-β, RA, or RA + TGF-β. (G) Heatmap showing expression of SI T_{RM} cell signature genes co-regulated by TGF-β, RA, and RA + TGF-β, as compared with Ctrl, as depicted in (F). (H) Bubble plot of log-odds ratios (LORs) and *p* values obtained from comparing transcriptional changes in SI T_{RM} cells vs. T_{CIRC} cells to those in TGF-β, RA, or RA + TGF-β-cultured CD8$^+$ T cells. Data are representative of 2 independent experiments with n = 2–3 samples (A, B and E–H) or n = 4 samples (C and D) per group.

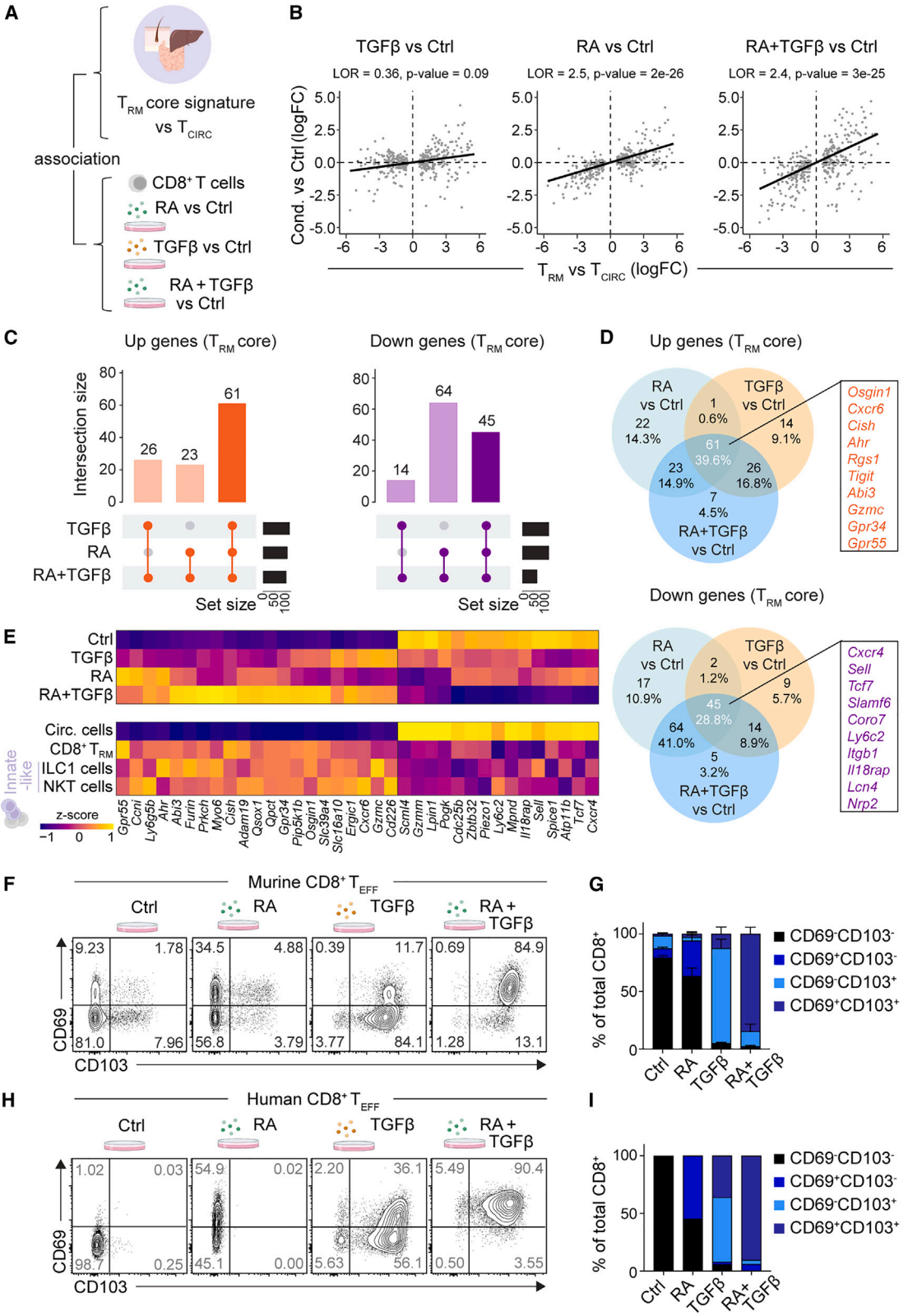

Figure 4. RA and TGF-β signals drive the shared tissue residency program

(A–E) Gene expression data from TGF-β, RA, or RA + TGF-β-cultured CD8+ T cells was compared with the core T_{RM} cell gene signature shared by skin, liver, and SI T_{RM} cells from GEO: GSE70813,[13] as depicted in (A). (B) Scatterplots showing gene expression changes for CD8+ T cells cultured with TGF-β, RA, or RA + TGF-

(legend continued on next page)

combined RA + TGF-β culture induced a transcriptional program that was more strongly correlated with the SI T_{RM} cell transcriptional profile compared with the effect of either factor in isolation (Figure 3H). In addition to these broad transcriptional changes, combining RA and TGF-β resulted in unique outcomes for several SI T_{RM} genes. For instance, we observed synergistic interactions between RA and TGF-β, elevating expression of several genes associated with the SI T_{RM} cell transcriptional program compared with that induced by each factor independently (Figure S3D). In addition, we identified a set of 126 genes from the SI T_{RM} cell gene signature that were uniquely regulated when both factors were present (Table S1). Together, these findings suggest that RA and TGF-β work synergistically to shape SI T_{RM} cell programming.

RA and TGF-β converge to instruct a shared tissue residency program

Although T_{RM} cells exhibit tissue-specific gene signatures, they share a common transcriptional foundation that is required to establish tissue residency.[11–13] Given the varied reliance of T_{RM} cells on either TGF-β or RA signals, we hypothesized that these extrinsic factors share an overlapping ability to drive common gene programs required for tissue residency. To investigate this, we compared the transcriptomes of $CD8^+$ T cells cultured with TGF-β or RA, or both factors combined, to the core transcriptional signature of T_{RM} cells derived from skin, SI, and liver versus T_{CIRC} cells[13] (Figure 4A). Additionally, we identified a significant association between RA-induced gene changes and the core T_{RM} cell signature, an effect that was further amplified when RA was combined with TGF-β (Figures 4B and S4A). RA and TGF-β also shared the ability to promote T_{RM} cell differentiation (via induction of *Ahr*, *Cxcr6*, *Rgs1,* and others)[35–37] and to reduce the expression of genes associated with T_{CIRC} cell commitment (e.g., *Ly6c2*, *Sell*, *Tcf7*, *Slamf6*, and *Cxcr4*) (Figures 4C and 4D).

Tissue residency extends beyond $CD8^+$ T cells to encompass innate-like lymphocytes, such as liver-residing group 1 innate lymphoid cells (ILC1) and natural killer T (NKT) cells, with which they share a common transcriptional program.[13] Accordingly, we found that tissue residency genes induced in $CD8^+$ T cells by RA and/or TGF-β mirrored gene expression in liver ILC1 and NKT cells. In particular, both tissue factors promoted the expression of genes universally expressed by $CD8^+$ T_{RM} cells, liver ILC1, and NKT (e.g., *Cxcr6*, *Osgin1*, *Gpr34*, *Gpr55*, and *Cish*), while repressing genes associated with a circulating fate (e.g., *Cxcr4*, *Sell*, and *Tcf7*) (Figure 4E). Together, these results underscore the central role of RA in shaping tissue-resident transcriptional signatures across distinct immune cell lineages. Despite the shared ability of both factors to regulate genes of the core T_{RM} cell program, the action of RA was magnified in the presence of TGF-β, revealing their combinatorial footprint in driving the core tissue residency program.

RA and TGF-β conditioning drive phenotypic changes associated with SI T_{RM} cells

Given that RA and TGF-β synergize to shape both core and SI T_{RM}-specific cell differentiation programs, we next asked whether the combination of these factors could recapitulate the phenotypic maturation of $CD8^+$ T cells into T_{RM}-like cells *in vitro*. Using CD69 and CD103 as surrogate markers for SI T_{RM} cell programming, we found that RA and TGF-β individually drove the expression of either CD69 or CD103 on $CD8^+$ T cells, respectively (Figures 4F and 4G). Co-expression of CD69 and CD103 on the majority of cultured $CD8^+$ T cells was observed only when both factors were present (Figures 4F and 4G), which was also true for cultured human $CD8^+$ T cells (Figures 4H and 4I). To further investigate the extent to which RA- and TGF-β-conditioned $CD8^+$ T cells resembled bona fide SI T_{RM} populations, we used high-dimensional spectral cytometry to compare their protein expression profiles, focusing on markers characteristic of T_{RM} or T_{CIRC} cells (Figure S4C). Akin to bona fide T_{RM} cells, RA- and TGF-β-conditioned cells suppressed "circulation-associated" molecules (e.g., CD62L, Ly6C, and NKG2D) and induced "residency-associated" markers (e.g., CD38, CD39, CD73, and β7-integrin) *in vitro* (Figures S4C and S4D). Although *in vitro*-cultured $CD8^+$ T cells shared a close resemblance to splenic T_{CIRC} cells, pre-conditioning these cells with RA and TGF-β led them to adopt a SI T_{RM}-cell-like phenotype (Figure S4E). Collectively, these results underscore the ability of RA and TGF-β to imprint the $CD8^+$ T_{RM}-cell-associated phenotype.

RA signaling regulates the long-term maintenance of conventional intestinal lymphocytes

Our results so far uncovered RA as an alternative driver of tissue residency. Modulating RA signals during the effector phase (Figures 1K–1M and S5A–S5F) and disrupting the RA-RARα axis (Figures S2A–S2D) had a substantial impact on SI T_{RM} cell differentiation. However, because RA signaling controls SI homing molecules like CCR9, defective tissue entry might primarily hinder SI T_{RM} cell generation during RA signaling deficiency. To test this, we forced CCR9 expression in Ctrl and dnRARα P14 cells and evaluated SI T_{RM} development (Figure 5A). Although CCR9 overexpression enhanced T cell entry into the SI, dnRARα T_{RM} cells were still lost during the memory phase (Figures 5B and 5C), indicating that RA signaling deficiency affects SI T_{RM} cells beyond tissue homing. To determine whether sustained RA signaling was necessary for the maintenance of established T_{RM} populations, we infected mice containing naive

β vs. Ctrl (*y axis*) against T_{RM} cells vs. T_{CIRC} cells (*x axis*) for core T_{RM} cell signature genes. Black line represents least-squares regression line fitted to all points. (C) UpSet plots showing core T_{RM} cell signature genes derived from GEO: GSE70813 [13] shared with $CD8^+$ T cells cultured with TGF-β, RA, or RA + TGF-β. Genes with increased and decreased expression in the core T_{RM} cell signature are depicted in orange and purple, respectively. (D) Venn diagrams showing core T_{RM} cell signature genes shared with $CD8^+$ T cells cultured with TGF-β, RA, or RA + TGF-β. Genes with increased and decreased expression in the core T_{RM} cell signature are depicted in orange and purple, respectively. (E) Heatmap showing expression of DEGs co-regulated by TGF-β, RA, and RA + TGF-β from (D) in indicated populations.

(F–I) Murine (F and G) and human (H and I) effector $CD8^+$ T cells were cultured in the absence (Ctrl) or presence of TGF-β, RA, or RA + TGF-β for 7 days (mouse) or 21 days (human). (F and H) Representative flow cytometry plots and (G and I) quantification of CD69 and CD103 expression in $CD8^+$ T cells for indicated conditions. Data are representative of 2 independent experiments with n = 2–3 samples or n = 1 donor (H and I) per group. Bars represent the mean.

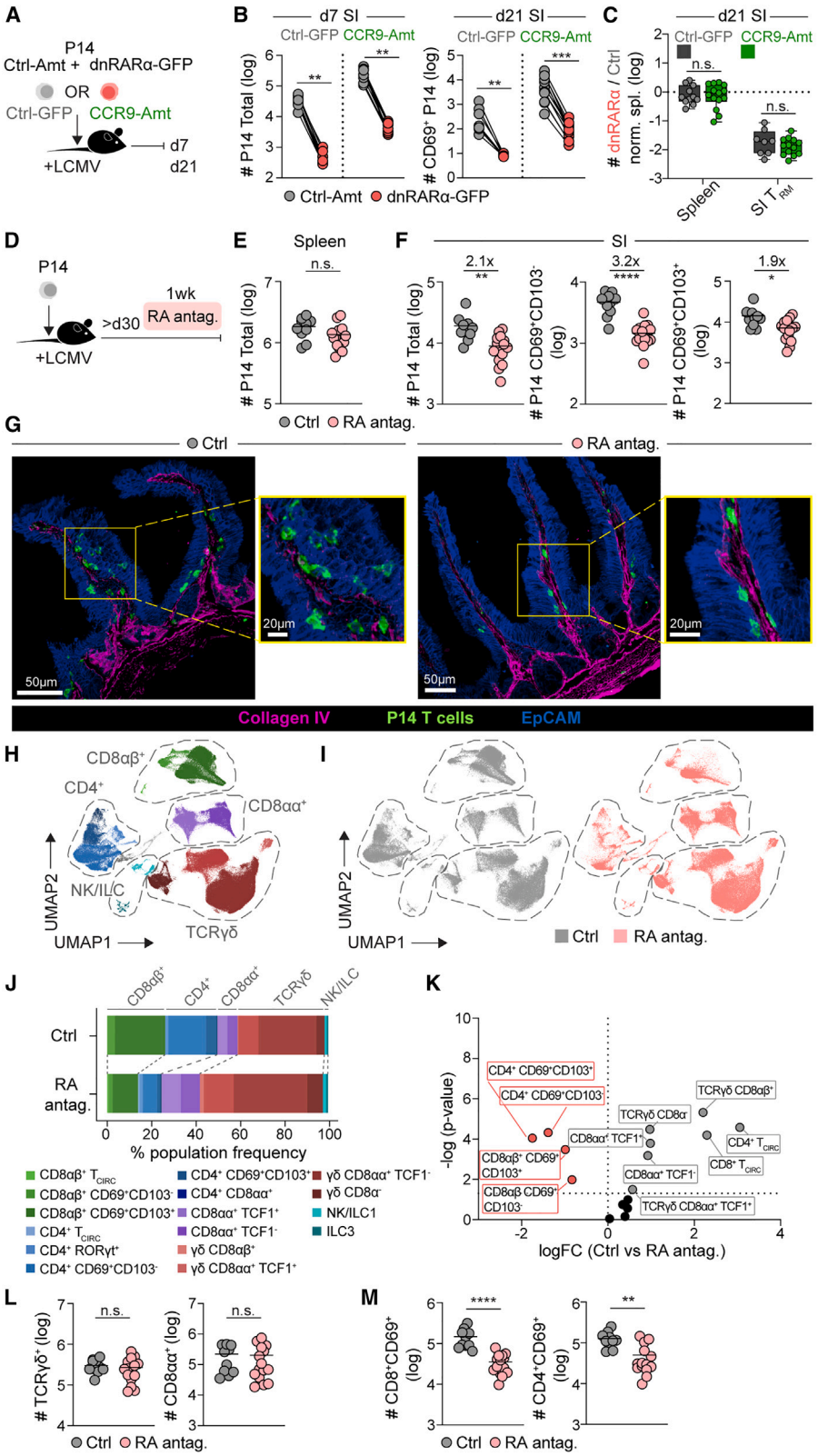

Figure 5. RA signals sustain adaptive cellular immunity in the intestine

(A–C) P14 cells were co-transduced with either control Ametrine (Ctrl-Amt) or dnRARα-GFP (dnRARα-GFP) retroviruses, as well as control-GFP (Ctrl-GFP) or CCR9 Ametrine (CCR9-Amt) retroviruses, were transferred into LCMV-infected recipient mice and isolated 7 and 21 days p.i., as depicted in (A). (B) Numbers of

(legend continued on next page)

P14 cells with LCMV and blocked RA signals for 7 days during the memory phase (>70 days p.i.). We found that inhibiting RA signaling after memory establishment resulted in a significant decline in P14 SI T_{RM} cells, leaving splenic T_{CIRC} unaltered (Figures 5D–5F). Although blocking RA signaling had a more dramatic impact on $CD69^+CD103^-$ T_{RM} cells compared with their $CD69^+CD103^+$ counterparts, an overall decline in total $CD69^+$ T_{RM} cells was observed irrespective of CD103 expression (Figure 5F). Additionally, immunofluorescence microscopy showed a reduced presence of P14 cells within the SI villi following RA antagonism (Figure 5G). Collectively, these results underscore the pivotal role of RA signaling in sustaining the SI T_{RM} cell compartment.

We next sought to investigate the impact of RA antagonism on the maintenance of other immune cell populations resident in the intestine, including conventional TCR$\alpha\beta$ $CD4^+$ and $CD8\alpha\beta^+$ T cells and unconventional TCR$\alpha\beta$ $CD8\alpha\alpha^+$ and TCR$\gamma\delta$ T cells, which are linked to tissue repair and homeostatic functions.[38] We found that inhibiting RA signaling caused a marked reduction in conventional TCR$\alpha\beta$ $CD4^+$ and $CD8\alpha\beta^+$ T cells expressing tissue residency markers (Figures 5H–5K and 5M). In contrast, unconventional TCR$\alpha\beta$ $CD8\alpha\alpha^+$ and TCR$\gamma\delta$ T cells numbers remained unaltered, resulting in a higher proportion of these cells in the SI of treated mice (Figures 5K and 5L). Thus, RA signaling is essential for maintaining $CD4^+$ and $CD8^+$ T_{RM} cells, whereas TCR$\alpha\beta$ $CD8\alpha\alpha^+$ and TCR$\gamma\delta$ cells appear to persist in the SI independently of RA signaling.

To understand the mechanism by which RA signaling promotes SI T_{RM} cell maintenance, we conducted RNA-seq analysis on SI T_{RM} cells following RA antagonist treatment (Figure S6A). We observed no significant changes in apoptosis-related molecules, such as Bcl2 and Bim, at both gene and protein level (Figures S6A–S6C). Additionally, we found that expression of the receptor P2RX7, which promotes SI T_{RM} cell survival and metabolic fitness,[39] was reduced upon RA signaling blockade (Figure S6D), consistent with a role for RA in P2RX7 expression.[40] However, P2RX7-ablated SI T_{RM} cells still decayed following RA antagonism (Figures S6E–S6G). Thus, SI T_{RM} cell loss did not appear to be linked to increased cell death *in situ*. Retrograde migration is a key mechanism by which T_{RM} cells decay in peripheral tissues.[41,42] Supporting this, RA antagonism resulted in increased expression of tissue egress genes (*Klf2*, *S1pr5*, *Zeb2*)[43] in SI T_{RM} cells (Figure S6B). To test whether T_{RM} cells leave the SI upon RA signaling blockade, we used a fate-mapping system based on the TF Hobit that is specifically expressed by T_{RM} cells (*Hobit*$^{cre\text{-}tdTomato}$:*Rosa26*$^{LsL\text{-}YFP}$) (Figures 6A and S6H) and was previously used to track T_{RM} cells and their progeny after antigen recall.[44] Using this system, we observed a decrease in SI T_{RM} cells and increase in SI "ex-T_{RM}" cells, along with a rise in T_{RM} and ex-T_{RM} cells in mesenteric LNs (mLNs) following RA signaling blockade, suggesting active migration away from the SI (Figures 6B and 6C). Furthermore, treatment with FTY720, which inhibits the S1P-signaling pathway and impedes tissue egress, alongside RA blockade, prevented the decrease in SI T_{RM} cells and the increase in mLN T cells (Figures 6D, 6E, S6I, and S6J). Supporting this, P14 cells were less frequently found within the SI epithelium, with some closely associated with lymphatics following RA signaling blockade (Figure 6F; Video S1). Collectively, these results indicate that sustained RA signaling promotes the long-term maintenance of SI T_{RM} cells by limiting their migration to draining LNs via the S1P signaling pathway.

RA replicates features of T_{RM} cells driven by microbial diversification

Tissue immune homeostasis requires an optimal balance of tissue-resident lymphocyte abundance and function. TGF-β can modulate the phenotype and function of T_{RM} cells,[17,37] raising the question of whether RA could exert similar effects. Following the temporal antagonism of RA signaling in naive mice, we found that endogenous $CD8^+$ T_{RM} cells isolated from the SI or liver exhibited reduced expression of the purinergic receptor P2RX7 and increased expression of memory-associated markers TCF-1 and CD127 (Figures 7A and 7B). Conversely, RA agonism enhanced P2RX7 expression and reduced TCF-1 and CD127 expression on these T_{RM} populations (Figures 7C and 7D), suggesting a multifaceted role of RA signaling in modulating both T_{RM} cell abundance and phenotype. Although RA is mainly produced by the host, the microbiota significantly contributes to RA production, either by metabolizing vitamin A and its derivatives or by directly producing RA.[45–47] Thus, we reasoned that T_{RM} cells found in mice with increased microbial experience may exhibit phenotypic features similar to those observed following RA agonism. To test this, we employed "dirty" mice that carry a diverse microbiome and an immune activation state more similar to adult humans.[48–52] We cohoused dirty mice with specific-pathogen-free (SPF) mice for 30 days, allowing their microbiome to equilibrate (Figures 7E, S7A, and S7B). This process allowed the introduction of various bacteria taxa in SPF mice, including *Lactobacillus* spp., which are known to produce RA[45] (Figures S7B and S7C). Consistent with this, microbial exposure increased RA levels in cohoused mice related to their SPF counterparts (Figure 7F). We did not observe an expansion of activated or memory $CD8^+$ T cells in the blood and spleen (Figures S7D and S7E), suggesting that systemic pathogen insults were limited in cohoused mice. Instead, we observed a pronounced shift of the SI immune landscape from unconventional to adaptive lymphocyte populations in microbially diverse

transduced (left) SI P14 cells at 7 days p.i. and (right) SI $CD69^+$ P14 cells at 21 days p.i. (C) Ratio of transduced Ctrl-Amt and dnRARα-GFP P14 cells in indicated tissues and experimental groups at 21 days p.i.

(D–M) Mice received P14 $Thy1.1^+$ cells and were infected with LCMV. At >30 days p.i., mice were treated with DMSO (Ctrl) or AGN194310 (RA antag.) for 6 days and were isolated from indicated tissues the following day as depicted in (D). (E and F) Enumeration of (E) splenic and (F) SI P14 cell populations in Ctrl or RA-antag.-treated mice. (G) Confocal microscopy images of SI showing collagen IV (magenta), P14 cells (Thy1.1, green), and epithelium (EpCAM, blue) in Ctrl and RA-antag.-treated mice. A zoomed-in view of P14 cells is shown (yellow inset). (H–K) Uniform manifold approximation and projection (UMAP) analysis of SI intraepithelial lymphocytes (SI-IELs). Cells were color-coded according to (H) lymphocyte lineages or (I) treatment. (J) Frequency and (K) volcano plot of lymphocyte subset abundance between Ctrl and treated groups. (L and M) Enumeration of (L) TCR$\gamma\delta^+$ and $CD8\alpha\alpha^+$ and (M) $CD8^+CD69^+$ and $CD4^+$ $CD69^+$ T cells from the SI >30 days p.i. Data are pooled from 2 to 3 independent experiments with $n = 5–15$ mice per group. $^*p \leq 0.05$, $^{**}p \leq 0.01$, $^{***}p \leq 0.001$, $^{****}p \leq 0.0001$, n.s., non-significant, Wilcoxon test (B), two-way ANOVA (C) or unpaired t test (D–M). Bars represent the mean; symbols represent individual mice.

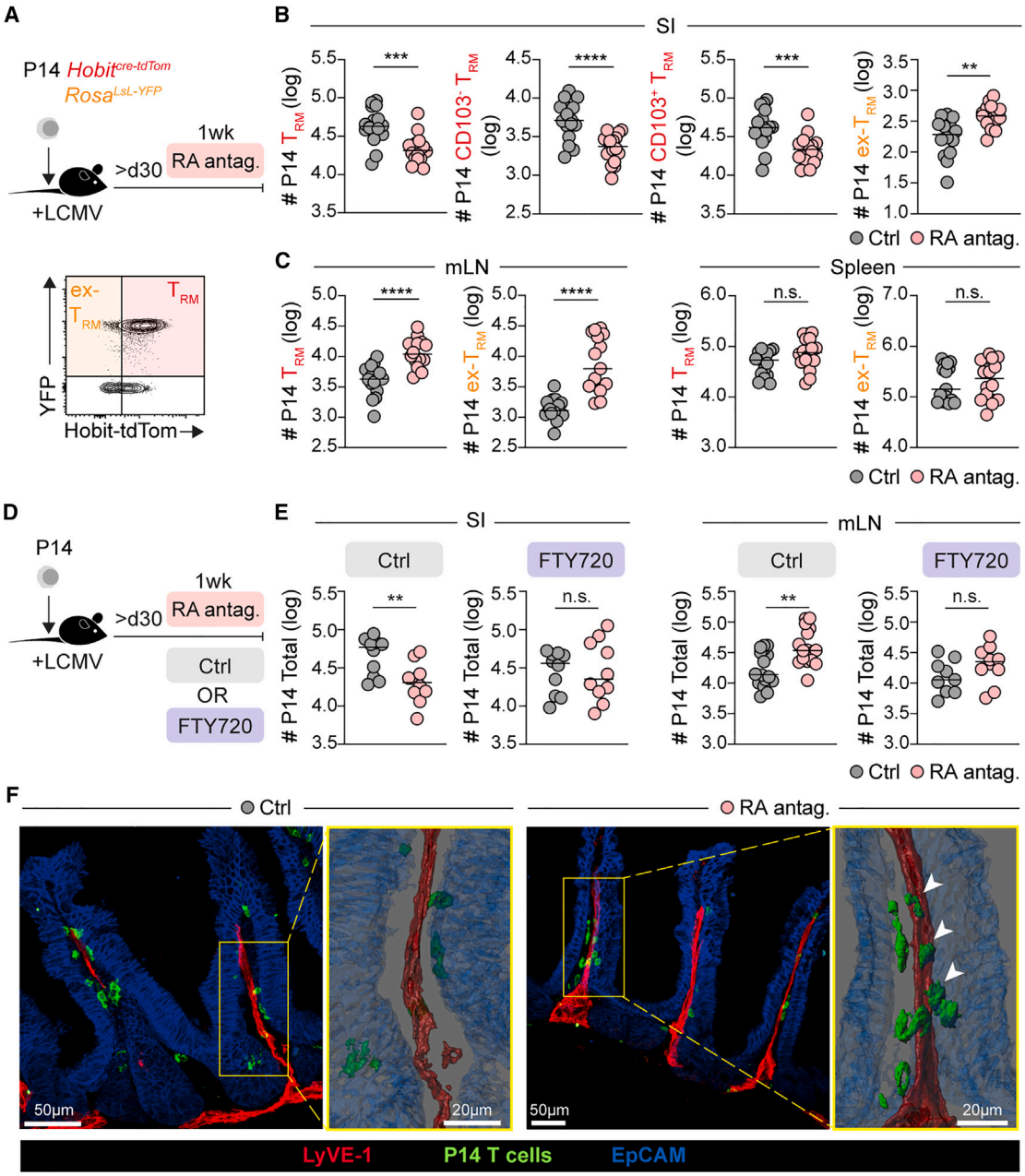

Figure 6. RA signals limit the retrograde migration of SI T_{RM} cells

(A–C) Mice received P14 *Hobit*$^{cre\text{-}tdTom}$:*Rosa26*$^{LsL\text{-}YFP}$ cells were transferred in LCMV-infected recipients. At >30 days p.i., mice were treated with DMSO (Ctrl) or AGN194310 (RA antag.) for 6 days and P14 cells were isolated from indicated tissues the following day, as depicted in (A). (B and C) Enumeration of P14 YFP$^+$TdTom$^+$ T_{RM} cells and P14 YFP$^+$TdTom$^-$ ex-T_{RM} cells isolated from indicated organs and treatment groups.

(D and E) P14 cells were transferred in LCMV-infected recipients. At >30 days p.i., mice were treated with DMSO or RA antag, while receiving FTY720 or cyclodextran (Ctrl) for 6 days, and P14 cells were isolated from indicated tissues the following day, as depicted in (D). (E) Enumeration of SI and mLN P14 cell populations for indicated treatment groups.

(F) P14 Thy1.1$^+$ cells and were infected with LCMV. At >30 days p.i., mice were treated with DMSO or RA antag. for 6 days and were sacrificed the following day. Confocal microscopy images of SI showing lymphatic endothelium (LyVE-1, red), P14 cells (Thy1.1, green) and epithelium (EpCAM, blue) in Ctrl and RA-antag.-treated mice. A zoomed-in three-dimensional [3D]-rendered view of P14 cells in relation to lymphatics and epithelium is shown (yellow inset). P14 cells in contact with lymphatics are depicted with arrowheads (white). Data are pooled from 2 to 3 independent experiments with n = 8–16 mice per group. $^{**}p \leq 0.01$, $^{***}p \leq 0.001$, $^{****}p \leq 0.0001$, n.s., non-significant, unpaired t test. Symbols represent individual mice.

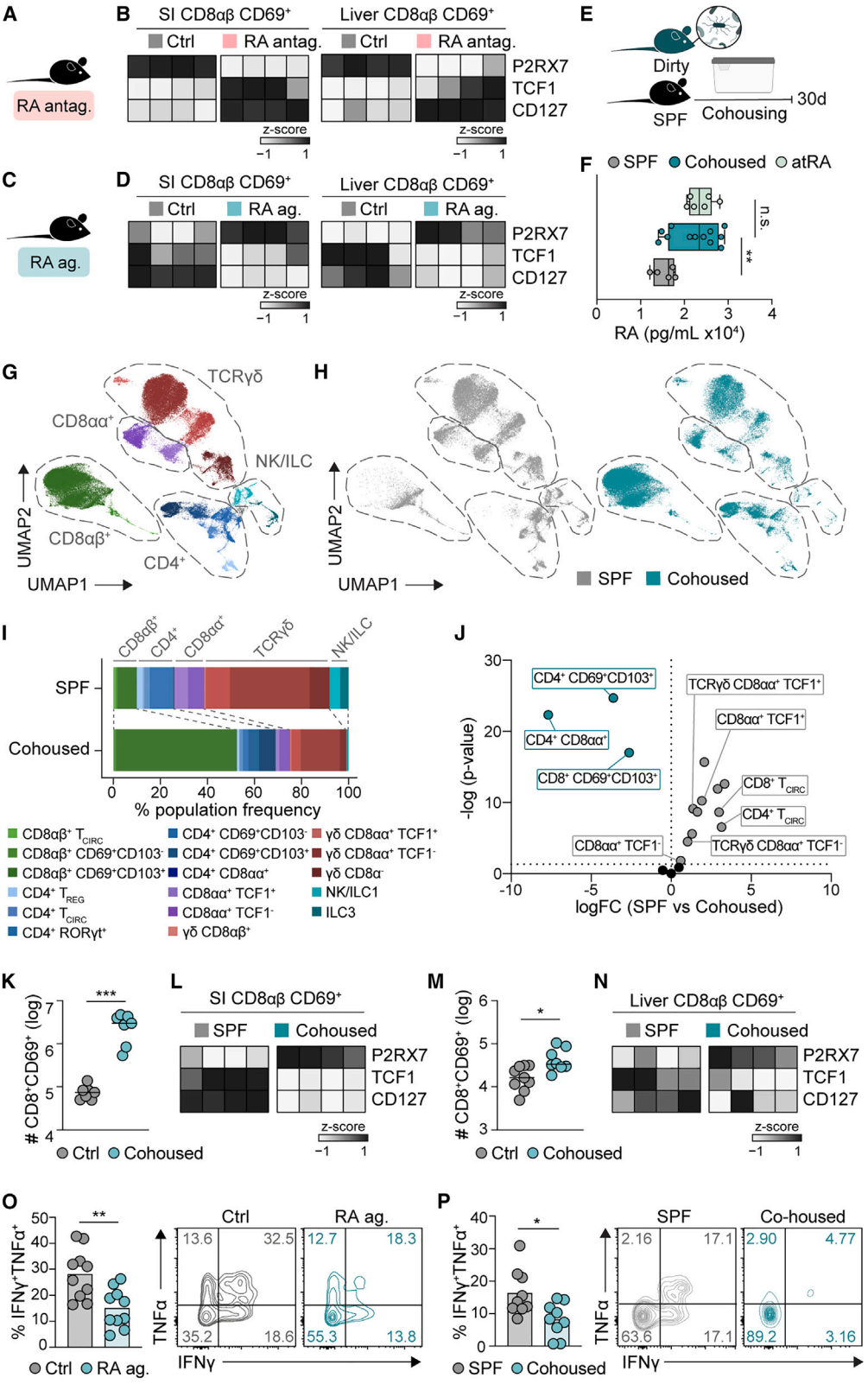

(legend on next page)

mice, with an increased abundance of conventional TCRαβ CD4$^+$ and CD8αβ$^+$ T cells expressing tissue residency markers, as well as the presence of CD4$^+$CD8αα$^+$ T cells (Figures 7G–7J and S7E), a population dependent on RA signaling for development.[53] In contrast, we noticed a concomitant decrease in the frequency of TCRαβ CD8αα$^+$ and TCRγδ T cells (Figures 7G–7J and S7E), the reverse of changes occurring after RA signaling blockade (Figures 6D–6G). Compared with SPF mice, conventional TCRαβ CD8$^+$ T_{RM} cells in both liver and SI of microbially diverse mice exhibited phenotypic changes that paralleled those observed after RA signaling agonism (Figures 7D and 7K–7N), implying that the augmented CD8$^+$ T_{RM} cell compartment and the altered phenotype of those cells upon microbial conditioning may be driven in part by increased RA signaling.

In addition to promoting CD8$^+$ T_{RM} cell development, we also noted that modulating RA signaling could impact T cell function, whereby disruption of RA signaling in dnRARα SI T_{RM} cells resulted in heightened production of pro-inflammatory cytokines interferon (IFN) γ and TNFα 21 days p.i (Figures S7F–S7H). Conversely, RA-agonized OT-I cells showed a reduced capacity to produce IFNγ and TNFα in the SI >30 days after transfer (Figures 7O and S7I–S7K). A similar decrease in CD8$^+$ T_{RM} cell functionality was evident after cohousing SPF mice with dirty mice for 30 days (Figure 7P), indicating that RA signaling and increased microbial exposure fine-tune the balance between the quantity and quality of CD8$^+$ T_{RM} cells, potentially minimizing tissue-damage at barrier sites exposed to external stimuli. Collectively, our data reveal the importance of RA signals in regulating the landscape of tissue-resident lymphocytes, acting as a bridge through which local immunity can be shaped in response to microbial diversity.

DISCUSSION

Tissue homeostasis relies on the strategic positioning of immune cells, including T_{RM} cells within tissues. Despite phenotypic diversity between organs, T_{RM} cells develop through a common transcriptional framework that enforces tissue residency. Paradoxically, this program operates in drastically different microenvironments, raising the question of how T cells integrate distinct cues to adopt a common T_{RM} cell fate. Although host-derived molecules, including TGF-β, are essential for tissue-resident lymphocyte programming in some organs, analogous factors remain poorly defined. Moreover, whether such tissue-derived cues can cooperate with microenvironmental factors to drive tissue residency was unresolved. Here, we reveal that RA shaped numerous aspects of tissue-resident lymphocyte biology, in part by collaborating with TGF-β. Beyond its role in T cell migration, we found that RA signaling altered T_{RM} cell phenotype, function, and durability. Lastly, enhancing RA signaling could mirror the tissue-resident lymphocyte landscape in mice with diversified microbiota, reflecting the complex interplay between local factors and environmental cues in regulating tissue immunity.

T_{RM} cell programming is orchestrated by transcriptional regulators and microenvironmental cues, which induce the retention and survival of T_{RM} precursor cells while suppressing T_{CIRC} cell differentiation.[11–13] Although this process results in a shared T_{RM} cell core signature across tissues, T_{RM} cells residing in individual tissues develop unique signatures that differentiate them from T_{CIRC} cells. Until now, the microenvironmental factors influencing these tissue-specific programs have remained elusive. Here, we show that T_{RM} cells exhibit distinct dependencies for TGF-β and RA signals, whereby skin and liver T_{RM} cells rely on either TGF-β or RA, respectively, and SI T_{RM} cells require both factors for development. Mechanistically, TGF-β and RA both induce genes essential for T_{RM} cell development and/or migration, including *Ahr*, *Cxcr6*, and *Rgs1*,[35–37] indicating that either factor is sufficient to drive core tissue residency programming. Nonetheless, TGF-β and RA also induced distinct gene sets unique to skin or liver T_{RM} cells, respectively, while their combined action shaped SI T_{RM} cell identity.

The divergent roles of TGF-β and RA may be attributable to their differing presence across tissues. Active TGF-β is abundant within epithelial microenvironments,[54] while RA bioavailability varies. RA precursors, such as retinol, are absorbed in the SI, stored in the liver, and redistributed to various body sites before local conversion into RA by epithelial, stromal, and dendritic cell (DC) populations.[46,55,56] Although RA is abundant in the SI and liver,[46,55,56] its availability in specific skin niches is unclear. Further work will determine whether skin T_{RM} cells exhibit an intrinsic defect in RA signaling pathways or lack access to RA signaling *in situ*.

Although RA signaling is crucial for inducing gut-homing molecules during T cell priming in SI draining LNs,[22,57] it also licenses SI T_{RM} cell differentiation prior to tissue entry.[58] Resonating with this, migratory DCs precondition naive T cells for T_{RM} cell differentiation by presenting active TGF-β in skin

Figure 7. RA imprinting typifies the T_{RM} cell landscape after microbial conditioning

(A–D) Mice were treated every other day with (A and B) DMSO (Ctrl) or AGN194310 (RA antag.) or (C and D) DMSO (Ctrl) or AM80 (RA ag.) for 7 days and endogenous CD8$^+$ T cells were isolated from the SI and liver, as depicted in (A and D). (B and D) Heatmap showing expression of P2RX7, TCF1, and CD127 in indicated populations and organs.

(E and F) Mice were housed in SPF conditions or cohoused with dirty mice for >30 days, as depicted in (E). (F) Serum RA concentrations of SPF, cohoused mice, or mice receiving all-*trans* retinoic acid (atRA) prior to sample collection determined by ELISA analysis.

(G–J) UMAP analysis of SI-IEL. Cells were color-coded according to (G) lymphocyte lineages or (H) treatment. (I) Frequency and (J) volcano plot of lymphocyte subset abundance between SPF and cohoused groups.

(K–N) Enumeration of endogenous CD8αβ CD69$^+$ T_{RM} cells isolated from the (K) SI or (M) liver from SPF or cohoused mice and (L and N) expression of indicated molecules depicted as a heatmap.

(O and P) (O) Mice received effector OT-I cells, were treated every other day with DMSO or RA ag. from 0 to 6 days post transfer and rested for >30 days.

(P) SPF mice received OT-I cells and were infected with Lm-OVA. At 30 days p.i., mice were kept in SPF conditions or cohoused with dirty mice for >30 days. (O and P) SI OT-I T cells were stimulated with OVA peptide and IFNγ and TNFα production was quantified. Shown is the percentage of IFNγ$^+$TNFα$^+$ among OT-I cells. Data are pooled from 2 to 3 independent experiments (F, M, O, and P) or representative of 2 independent experiments (B, D, G–J, K, L, and N) with n = 4–7 mice (B, D, F–J, K, L, and N) or with n = 8–10 samples (F, M, O, and P), $^*p \leq 0.05$, $^{**}p \leq 0.01$, $^{***}p \leq 0.001$, unpaired t test. Bars represent the mean, symbols represent individual mice.

draining LNs.[59] Because DCs produce TGF-β and RA,[56,57] these molecules could synergize during T cell priming, with this effect being potentially amplified when T_{RM} precursor cells undergo maturation in the SI. Interestingly, the combined actions of TGF-β and RA extend beyond $CD8^+$ T cells, shaping the differentiation of multiple lymphocyte populations in the SI.[21,53,60,61] In particular, the combination of TGF-β and RA is essential for establishing oral tolerance by favoring peripheral Treg cell development over Th17 cells.[21] Although this synergy seems primarily confined to the SI, TGF-β or RA may interface with additional local factors to drive tissue-specific T_{RM} differentiation in other locations.

T_{RM} cells confer prolonged immune protection by persisting in peripheral tissues. At epithelial sites, continuous microenvironmental signals, such as TGF-β, are crucial for T_{RM} cell longevity.[31,62] Mechanistically, purinergic signaling through P2RX7 or CD38 enhances TGF-β sensitivity in T_{RM} cells, thereby supporting their maintenance.[39,63] Unlike TGF-β, sustained RA signaling is essential for retaining SI T_{RM} cells locally by limiting their retrograde migration. Although this migration pattern was observed early during T_{RM} cell differentiation (<20 days p.i.)[41,42] or in mature T_{RM} cells following antigen recall,[44] our study demonstrates that this process can also occur long after antigen clearance (>70 days p.i.). Furthermore, retrograde migration induced by interrupted RA signaling predominantly affects the $CD103^-$ T_{RM} cell population, which can robustly expand during secondary infections.[64,65] As RA levels can fluctuate during infections,[66–68] these fluctuations may prompt SI T_{RM} cells to retreat to draining LNs and mount effective mucosal responses.

Vitamin A deficiency is a prevalent cause of nutrient deficiency linked with impaired adaptive immunity,[69,70] in line with our data highlighting that RA is required for the abundance and maintenance of $CD8^+$ T_{RM} cells in specific organs. Considering the significant correlation between T_{RM} cell density and immune defense,[26,71,72] the loss of T_{RM} cells during vitamin A deficiency is likely to compromise immune protection. In addition to dietary effects, altered microbial diversity reshapes the adaptive immune compartment,[48,50,51] whereas unconventional T cells remain numerically stable, as seen in germ-free mice.[73,74] Interestingly, we found that both RA and microbial diversity diminished pro-inflammatory cytokine production in T_{RM} cells, consistent with observations that microbially enriched mice exhibit compromised adaptive immune responses after influenza infection.[51] Although this loss of protection could be tissue and context specific, it highlights the balance between increased T_{RM} cell numbers and restricted cytokine production to prevent excessive immune activation, potentially compromising pathogen control.

Together, our work highlights RA as a key orchestrator of immunological memory, coordinating multiple aspects of T cell biology within peripheral organs, from tissue residency programming to effector function. Harnessing the potential of RA through cell conditioning or microbiota manipulation may enhance the generation of protective T_{RM} cells or eliminate autoimmune tissue-resident populations, optimizing local immunity and improving disease outcomes.

Limitations of the study

Our study primarily employed T cell receptor (TCR) transgenic $CD8^+$ T cells in the context of LCMV infection, which generate a $T_{RM}1$-biased population that do not fully capture the diversity of $CD8^+$ T cell responses.[75] As such, the contribution of RA signaling to non-canonical endogenous responses such as $T_{RM}17$ was not investigated. Additionally, we used an antagonist to study the impact of RA signaling on T_{RM} cell maintenance, and thus it remains unclear whether the observed effects are intrinsic to T_{RM} cells or mediated indirectly through other cell types. Although we showed that RA blockade prompts the retrograde migration of SI T_{RM} cells, a fraction of these cells may undergo apoptosis in the lamina propria before reaching draining LNs. Finally, although RA-producing taxa like Lactobacillus were more abundant in cohoused mice, other unidentified bacteria likely produce RA additional microbial species and metabolites could contribute to the observed changes in T_{RM} cells beyond RA signaling.

RESOURCE AVAILABILITY

Lead contact

Further information and requests for resources and reagents should be directed to and will be fulfilled by Laura Mackay (lkmackay@unimelb.edu.au) upon reasonable request.

Materials availability

Plasmids generated in this study are available from the lead contact upon request.

Data and code availability

All data have been deposited at GEO: GSE232852, GSE277120, GSE277247, and GSE277248; BioProject: PRJNA1153786, and are publicly available as of the date of publication. Accession numbers are listed in the key resources table.

This paper does not report original code.

Any additional information required to reanalyze the data reported in this paper is available from the lead contact upon request.

ACKNOWLEDGMENTS

We thank Brooke Davies, Keely McDonald, and Natasha Zamudio for expert technical assistance. We thank the Melbourne Cytometry Platform from the Peter Doherty Institute for assistance with cell sorting. We thank the University of Melbourne's Biological Optical Microscopy Platform (BOMP) for their support and assistance. This work was supported by a Howard Hughes Medical Institute and Bill and Melinda Gates Foundation International Research Scholarship OPP1175796 to L.K.M. M.E. and R.F. are supported by an ARC DECRA Fellowship. T.G.P. is supported by NHMRC Senior Research Fellowship 1155678, investigator grant 2026122, and project grant 1139865. S.L.P. is supported by a Cancer Research Institute Postdoctoral Fellowship. L.K.M. is a senior medical research fellow supported by Sylvia and Charles Viertel Charitable Foundation Fellowship VIERSMRF2018045 and NHMRC Leadership Investigator Grant GNT1178498.

AUTHOR CONTRIBUTIONS

Conceptualization, A.O., C.Z., M.E., and L.K.M.; investigation, A.O., T.P., G.R., S.N.C., A.Z., J.E.Y.K., H.L., P.Z., T.N.B., J.D., F.A.B., C.A.L., C.W., L.J., M.R.T., and M.E.; formal analysis, A.O., T.P., L.C.G., R.F. A.Z., L.D., F.A.B., C.W., and M.E.; software, L.C.G., R.F., and M.E.; writing original draft, A.O., M.E., and L.K.M.; writing – review and editing, A.O., S.N.M., S.L.P., M.E., and L.K.M.; visualization, A.O., M.E., M.H.Y. and L.K.M.; resources, K.G., P.D., J.K., and T.G.P.; funding acquisition, C.Z. and L.K.M.; supervision T.S., J.S., T.P.S., A.T.S., C.Z., C.W., M.E., and L.K.M.

DECLARATION OF INTERESTS

The authors declare no competing interests.

STAR★METHODS

Detailed methods are provided in the online version of this paper and include the following:

- KEY RESOURCES TABLE
- EXPERIMENTAL MODEL AND SUBJECT DETAILS
  - Mice
  - T cell transfer
  - Infections and DNFB treatment
  - *In vivo* treatments
  - Mouse tissue processing
  - Flow cytometry
  - T cell stimulations and cytokine staining
  - Flow cytometry high dimensional analyses
  - Immunofluorescence and confocal microscopy
  - Retinoic acid quantification
  - CRISPR/Cas9 gene editing of $CD8^+$ T cells
  - Retroviral transduction of CD8+ T cells
  - ATAC-seq
  - RNA-seq
  - 16S rRNA-seq
- QUANTIFICATION AND STATISTICAL ANALYSIS

SUPPLEMENTAL INFORMATION

Supplemental information can be found online at https://doi.org/10.1016/j.immuni.2024.09.015.

Received: May 21, 2023
Revised: July 23, 2024
Accepted: September 21, 2024
Published: October 14, 2024

REFERENCES

1. Mayassi, T., Barreiro, L.B., Rossjohn, J., and Jabri, B. (2021). A multilayered immune system through the lens of unconventional T cells. Nature *595*, 501–510. https://doi.org/10.1038/s41586-021-03578-0.
2. Fan, X., and Rudensky, A.Y. (2016). Hallmarks of Tissue-Resident Lymphocytes. Cell *164*, 1198–1211. https://doi.org/10.1016/j.cell.2016.02.048.
3. Klose, C.S.N., and Artis, D. (2016). Innate lymphoid cells as regulators of immunity, inflammation and tissue homeostasis. Nat. Immunol. *17*, 765–774. https://doi.org/10.1038/ni.3489.
4. Park, M.D., Silvin, A., Ginhoux, F., and Merad, M. (2022). Macrophages in health and disease. Cell *185*, 4259–4279. https://doi.org/10.1016/j.cell.2022.10.007.
5. Park, C.O., and Kupper, T.S. (2015). The emerging role of resident memory T cells in protective immunity and inflammatory disease. Nat. Med. *21*, 688–697. https://doi.org/10.1038/nm.3883.
6. Sasson, S.C., Gordon, C.L., Christo, S.N., Klenerman, P., and Mackay, L.K. (2020). Local heroes or villains: tissue-resident memory T cells in human health and disease. Cell. Mol. Immunol. *17*, 113–122. https://doi.org/10.1038/s41423-019-0359-1.
7. Amsen, D., van Gisbergen, K.P.J.M., Hombrink, P., and van Lier, R.A.W. (2018). Tissue-resident memory T cells at the center of immunity to solid tumors. Nat. Immunol. *19*, 538–546. https://doi.org/10.1038/s41590-018-0114-2.
8. Masopust, D., and Soerens, A.G. (2019). Tissue-Resident T Cells and Other Resident Leukocytes. Annu. Rev. Immunol. *37*, 521–546. https://doi.org/10.1146/annurev-immunol-042617-053214.
9. Collins, N., and Belkaid, Y. (2022). Control of immunity via nutritional interventions. Immunity *55*, 210–223. https://doi.org/10.1016/j.immuni.2022.01.004.
10. Lavin, Y., Mortha, A., Rahman, A., and Merad, M. (2015). Regulation of macrophage development and function in peripheral tissues. Nat. Rev. Immunol. *15*, 731–744. https://doi.org/10.1038/nri3920.
11. Mackay, L.K., Rahimpour, A., Ma, J.Z., Collins, N., Stock, A.T., Hafon, M.L., Vega-Ramos, J., Lauzurica, P., Mueller, S.N., Stefanovic, T., et al. (2013). The developmental pathway for CD103(+)CD8+ tissue-resident memory T cells of skin. Nat. Immunol. *14*, 1294–1301. https://doi.org/10.1038/ni.2744.
12. Milner, J.J., Toma, C., Yu, B., Zhang, K., Omilusik, K., Phan, A.T., Wang, D., Getzler, A.J., Nguyen, T., Crotty, S., et al. (2017). Runx3 programs $CD8^+$ T cell residency in non-lymphoid tissues and tumours. Nature *552*, 253–257. https://doi.org/10.1038/nature24993.
13. Mackay, L.K., Minnich, M., Kragten, N.A.M., Liao, Y., Nota, B., Seillet, C., Zaid, A., Man, K., Preston, S., Freestone, D., et al. (2016). Hobit and Blimp1 instruct a universal transcriptional program of tissue residency in lymphocytes. Science *352*, 459–463. https://doi.org/10.1126/science.aad2035.
14. Mackay, L.K., Wynne-Jones, E., Freestone, D., Pellicci, D.G., Mielke, L.A., Newman, D.M., Braun, A., Masson, F., Kallies, A., Belz, G.T., et al. (2015). T-box Transcription Factors Combine with the Cytokines TGF-beta and IL-15 to Control Tissue-Resident Memory T Cell Fate. Immunity *43*, 1101–1111. https://doi.org/10.1016/j.immuni.2015.11.008.
15. Casey, K.A., Fraser, K.A., Schenkel, J.M., Moran, A., Abt, M.C., Beura, L.K., Lucas, P.J., Artis, D., Wherry, E.J., Hogquist, K., et al. (2012). Antigen-independent differentiation and maintenance of effector-like resident memory T cells in tissues. J. Immunol. *188*, 4866–4875. https://doi.org/10.4049/jimmunol.1200402.
16. Zhang, N., and Bevan, M.J. (2013). Transforming growth factor-beta signaling controls the formation and maintenance of gut-resident memory T cells by regulating migration and retention. Immunity *39*, 687–696. https://doi.org/10.1016/j.immuni.2013.08.019.
17. Christo, S.N., Evrard, M., Park, S.L., Gandolfo, L.C., Burn, T.N., Fonseca, R., Newman, D.M., Alexandre, Y.O., Collins, N., Zamudio, N.M., et al. (2021). Discrete tissue microenvironments instruct diversity in resident memory T cell function and plasticity. Nat. Immunol. *22*, 1140–1151. https://doi.org/10.1038/s41590-021-01004-1.
18. Belkaid, Y., and Harrison, O.J. (2017). Homeostatic Immunity and the Microbiota. Immunity *46*, 562–576. https://doi.org/10.1016/j.immuni.2017.04.008.
19. Mowat, A.M., and Agace, W.W. (2014). Regional specialization within the intestinal immune system. Nat. Rev. Immunol. *14*, 667–685. https://doi.org/10.1038/nri3738.
20. Hang, S., Paik, D., Yao, L., Kim, E., Trinath, J., Lu, J., Ha, S., Nelson, B.N., Kelly, S.P., Wu, L., et al. (2019). Bile acid metabolites control T_H17 and T_{reg} cell differentiation. Nature *576*, 143–148. https://doi.org/10.1038/s41586-019-1785-z.
21. Mucida, D., Park, Y., Kim, G., Turovskaya, O., Scott, I., Kronenberg, M., and Cheroutre, H. (2007). Reciprocal TH17 and regulatory T cell differentiation mediated by retinoic acid. Science *317*, 256–260. https://doi.org/10.1126/science.1145697.
22. Iwata, M., Hirakiyama, A., Eshima, Y., Kagechika, H., Kato, C., and Song, S.Y. (2004). Retinoic acid imprints gut-homing specificity on T cells. Immunity *21*, 527–538. https://doi.org/10.1016/j.immuni.2004.08.011.
23. Joshi, N.S., Cui, W., Chandele, A., Lee, H.K., Urso, D.R., Hagman, J., Gapin, L., and Kaech, S.M. (2007). Inflammation directs memory precursor and short-lived effector CD8(+) T cell fates via the graded expression of T-bet transcription factor. Immunity *27*, 281–295. https://doi.org/10.1016/j.immuni.2007.07.010.
24. Laidlaw, B.J., Zhang, N., Marshall, H.D., Staron, M.M., Guan, T., Hu, Y., Cauley, L.S., Craft, J., and Kaech, S.M. (2014). CD4+ T cell help guides formation of CD103+ lung-resident memory CD8+ T cells during influenza viral infection. Immunity *41*, 633–645. https://doi.org/10.1016/j.immuni.2014.09.007.
25. Schenkel, J.M., Fraser, K.A., Casey, K.A., Beura, L.K., Pauken, K.E., Vezys, V., and Masopust, D. (2016). IL-15-Independent Maintenance of

Tissue-Resident and Boosted Effector Memory CD8 T Cells. J. Immunol. *196*, 3920–3926. https://doi.org/10.4049/jimmunol.1502337.

26. Sheridan, B.S., Pham, Q.M., Lee, Y.T., Cauley, L.S., Puddington, L., and Lefrançois, L. (2014). Oral infection drives a distinct population of intestinal resident memory CD8(+) T cells with enhanced protective function. Immunity *40*, 747–757. https://doi.org/10.1016/j.immuni.2014.03.007.
27. Li, C., Zhu, B., Son, Y.M., Wang, Z., Jiang, L., Xiang, M., Ye, Z., Beckermann, K.E., Wu, Y., Jenkins, J.W., et al. (2019). The Transcription Factor Bhlhe40 Programs Mitochondrial Regulation of Resident CD8$^+$ T Cell Fitness and Functionality. Immunity *51*, 491–507.e7. https://doi.org/10.1016/j.immuni.2019.08.013.
28. Buquicchio, F.A., Fonseca, R., Belk, J.A., Evrard, M., Obers, A., Qi, Y., Daniel, B., Yost, K.E., Satpathy, A.T., and Mackay, L.K. (2022). A unique epigenomic landscape defines CD8+ tissue-resident memory T cells. Preprint at bioRxiv. https://doi.org/10.1101/2022.05.04.490680.
29. Milner, J.J., Toma, C., He, Z., Kurd, N.S., Nguyen, Q.P., McDonald, B., Quezada, L., Widjaja, C.E., Witherden, D.A., Crowl, J.T., et al. (2020). Heterogenous Populations of Tissue-Resident CD8$^+$ T Cells Are Generated in Response to Infection and Malignancy. Immunity *52*, 808–824.e7. https://doi.org/10.1016/j.immuni.2020.04.007.
30. Burrows, K., Antignano, F., Bramhall, M., Chenery, A., Scheer, S., Korinek, V., Underhill, T.M., and Zaph, C. (2017). The transcriptional repressor HIC1 regulates intestinal immune homeostasis. Mucosal Immunol. *10*, 1518–1528. https://doi.org/10.1038/mi.2017.17.
31. Crowl, J.T., Heeg, M., Ferry, A., Milner, J.J., Omilusik, K.D., Toma, C., He, Z., Chang, J.T., and Goldrath, A.W. (2022). Tissue-resident memory CD8$^+$ T cells possess unique transcriptional, epigenetic and functional adaptations to different tissue environments. Nat. Immunol. *23*, 1121–1131. https://doi.org/10.1038/s41590-022-01229-8.
32. Damm, K., Heyman, R.A., Umesono, K., and Evans, R.M. (1993). Functional inhibition of retinoic acid response by dominant negative retinoic acid receptor mutants. Proc. Natl. Acad. Sci. USA *90*, 2989–2993. https://doi.org/10.1073/pnas.90.7.2989.
33. Frizzell, H., Fonseca, R., Christo, S.N., Evrard, M., Cruz-Gomez, S., Zanluqui, N.G., von Scheidt, B., Freestone, D., Park, S.L., McWilliam, H.E.G., et al. (2020). Organ-specific isoform selection of fatty acid-binding proteins in tissue-resident lymphocytes. Sci. Immunol. *5*, eaay9283. https://doi.org/10.1126/sciimmunol.aay9283.
34. Allie, S.R., Zhang, W., Tsai, C.Y., Noelle, R.J., and Usherwood, E.J. (2013). Critical role for all-trans retinoic acid for optimal effector and effector memory CD8 T cell differentiation. J. Immunol. *190*, 2178–2187. https://doi.org/10.4049/jimmunol.1201945.
35. Wein, A.N., McMaster, S.R., Takamura, S., Dunbar, P.R., Cartwright, E.K., Hayward, S.L., McManus, D.T., Shimaoka, T., Ueha, S., Tsukui, T., et al. (2019). CXCR6 regulates localization of tissue-resident memory CD8 T cells to the airways. J. Exp. Med. *216*, 2748–2762. https://doi.org/10.1084/jem.20181308.
36. Zaid, A., Mackay, L.K., Rahimpour, A., Braun, A., Veldhoen, M., Carbone, F.R., Manton, J.H., Heath, W.R., and Mueller, S.N. (2014). Persistence of skin-resident memory T cells within an epidermal niche. Proc. Natl. Acad. Sci. USA *111*, 5307–5312. https://doi.org/10.1073/pnas.1322292111.
37. von Werdt, D., Gungor, B., Barreto de Albuquerque, J., Gruber, T., Zysset, D., Kwong Chung, C.K.C., Corrêa-Ferreira, A., Berchtold, R., Page, N., Schenk, M., et al. (2023). Regulator of G-protein signaling 1 critically supports CD8$^+$ T_{RM} cell-mediated intestinal immunity. Front. Immunol. *14*, 1085895. https://doi.org/10.3389/fimmu.2023.1085895.
38. McDonald, B.D., Jabri, B., and Bendelac, A. (2018). Diverse developmental pathways of intestinal intraepithelial lymphocytes. Nat. Rev. Immunol. *18*, 514–525. https://doi.org/10.1038/s41577-018-0013-7.
39. Borges da Silva, H., Peng, C., Wang, H., Wanhainen, K.M., Ma, C., Lopez, S., Khoruts, A., Zhang, N., and Jameson, S.C. (2020). Sensing of ATP via the Purinergic Receptor P2RX7 Promotes CD8$^+$ Trm Cell Generation by Enhancing Their Sensitivity to the Cytokine TGF-β. Immunity *53*, 158–171.e6. https://doi.org/10.1016/j.immuni.2020.06.010.
40. Hashimoto-Hill, S., Friesen, L., Kim, M., and Kim, C.H. (2017). Contraction of intestinal effector T cells by retinoic acid-induced purinergic receptor P2X7. Mucosal Immunol. *10*, 912–923. https://doi.org/10.1038/mi.2016.109.
41. Heim, T.A., Schultz, A.C., Delclaux, I., Cristaldi, V., Churchill, M.J., Ventre, K.S., and Lund, A.W. (2024). Lymphatic vessel transit seeds cytotoxic resident memory T cells in skin draining lymph nodes. Sci. Immunol. *9*, eadk8141. https://doi.org/10.1126/sciimmunol.adk8141.
42. Stolley, J.M., Johnston, T.S., Soerens, A.G., Beura, L.K., Rosato, P.C., Joag, V., Wijeyesinghe, S.P., Langlois, R.A., Osum, K.C., Mitchell, J.S., et al. (2020). Retrograde migration supplies resident memory T cells to lung-draining LN after influenza infection. J. Exp. Med. *217*, e20192197. https://doi.org/10.1084/jem.20192197.
43. Evrard, M., Wynne-Jones, E., Peng, C., Kato, Y., Christo, S.N., Fonseca, R., Park, S.L., Burn, T.N., Osman, M., Devi, S., et al. (2022). Sphingosine 1-phosphate receptor 5 (S1PR5) regulates the peripheral retention of tissue-resident lymphocytes. J. Exp. Med. *219*, 20210116. https://doi.org/10.1084/jem.20210116.
44. Behr, F.M., Parga-Vidal, L., Kragten, N.A.M., van Dam, T.J.P., Wesselink, T.H., Sheridan, B.S., Arens, R., van Lier, R.A.W., Stark, R., and van Gisbergen, K.P.J.M. (2020). Tissue-resident memory CD8$^+$ T cells shape local and systemic secondary T cell responses. Nat. Immunol. *21*, 1070–1081. https://doi.org/10.1038/s41590-020-0723-4.
45. Bonakdar, M., Czuba, L.C., Han, G., Zhong, G., Luong, H., Isoherranen, N., and Vaishnava, S. (2022). Gut commensals expand vitamin A metabolic capacity of the mammalian host. Cell Host Microbe *30*, 1084–1092.e5. https://doi.org/10.1016/j.chom.2022.06.011.
46. Hall, J.A., Grainger, J.R., Spencer, S.P., and Belkaid, Y. (2011). The role of retinoic acid in tolerance and immunity. Immunity *35*, 13–22. https://doi.org/10.1016/j.immuni.2011.07.002.
47. Woo, V., Eshleman, E.M., Hashimoto-Hill, S., Whitt, J., Wu, S.E., Engleman, L., Rice, T., Karns, R., Qualls, J.E., Haslam, D.B., et al. (2021). Commensal segmented filamentous bacteria-derived retinoic acid primes host defense to intestinal infection. Cell Host Microbe *29*, 1744–1756.e5. https://doi.org/10.1016/j.chom.2021.09.010.
48. Beura, L.K., Hamilton, S.E., Bi, K., Schenkel, J.M., Odumade, O.A., Casey, K.A., Thompson, E.A., Fraser, K.A., Rosato, P.C., Filali-Mouhim, A., et al. (2016). Normalizing the environment recapitulates adult human immune traits in laboratory mice. Nature *532*, 512–516. https://doi.org/10.1038/nature17655.
49. Rosshart, S.P., Herz, J., Vassallo, B.G., Hunter, A., Wall, M.K., Badger, J.H., McCulloch, J.A., Anastasakis, D.G., Sarshad, A.A., Leonardi, I., et al. (2019). Laboratory mice born to wild mice have natural microbiota and model human immune responses. Science *365*, eaaw4361. https://doi.org/10.1126/science.aaw4361.
50. Yeung, F., Chen, Y.H., Lin, J.D., Leung, J.M., McCauley, C., Devlin, J.C., Hansen, C., Cronkite, A., Stephens, Z., Drake-Dunn, C., et al. (2020). Altered Immunity of Laboratory Mice in the Natural Environment Is Associated with Fungal Colonization. Cell Host Microbe *27*, 809–822.e6. https://doi.org/10.1016/j.chom.2020.02.015.
51. Fiege, J.K., Block, K.E., Pierson, M.J., Nanda, H., Shepherd, F.K., Mickelson, C.K., Stolley, J.M., Matchett, W.E., Wijeyesinghe, S., Meyerholz, D.K., et al. (2021). Mice with diverse microbial exposure histories as a model for preclinical vaccine testing. Cell Host Microbe *29*, 1815–1827.e6. https://doi.org/10.1016/j.chom.2021.10.001.
52. Hamilton, S.E., Badovinac, V.P., Beura, L.K., Pierson, M., Jameson, S.C., Masopust, D., and Griffith, T.S. (2020). New Insights into the Immune System Using Dirty Mice. J. Immunol. *205*, 3–11. https://doi.org/10.4049/jimmunol.2000171.
53. Reis, B.S., Rogoz, A., Costa-Pinto, F.A., Taniuchi, I., and Mucida, D. (2013). Mutual expression of the transcription factors Runx3 and ThPOK regulates intestinal CD4$^+$ T cell immunity. Nat. Immunol. *14*, 271–280. https://doi.org/10.1038/ni.2518.
54. McEntee, C.P., Gunaltay, S., and Travis, M.A. (2020). Regulation of barrier immunity and homeostasis by integrin-mediated transforming growth

factor beta activation. Immunology *160*, 139–148. https://doi.org/10.1111/imm.13162.

55. Bono, M.R., Tejon, G., Flores-Santibañez, F., Fernandez, D., Rosemblatt, M., and Sauma, D. (2016). Retinoic Acid as a Modulator of T Cell Immunity. Nutrients *8*, 349. https://doi.org/10.3390/nu8060349.
56. Jaensson-Gyllenbäck, E., Kotarsky, K., Zapata, F., Persson, E.K., Gundersen, T.E., Blomhoff, R., and Agace, W.W. (2011). Bile retinoids imprint intestinal CD103+ dendritic cells with the ability to generate gut-tropic T cells. Mucosal Immunol. *4*, 438–447. https://doi.org/10.1038/mi.2010.91.
57. Johansson-Lindbom, B., Svensson, M., Pabst, O., Palmqvist, C., Marquez, G., Förster, R., and Agace, W.W. (2005). Functional specialization of gut CD103+ dendritic cells in the regulation of tissue-selective T cell homing. J. Exp. Med. *202*, 1063–1073. https://doi.org/10.1084/jem.20051100.
58. Qiu, Z., Khairallah, C., Chu, T.H., Imperato, J.N., Lei, X., Romanov, G., Atakilit, A., Puddington, L., and Sheridan, B.S. (2023). Retinoic acid signaling during priming licenses intestinal CD103+ CD8 TRM cell differentiation. J. Exp. Med. *220*, e20210923. https://doi.org/10.1084/jem.20210923.
59. Mani, V., Bromley, S.K., Äijö, T., Mora-Buch, R., Carrizosa, E., Warner, R.D., Hamze, M., Sen, D.R., Chasse, A.Y., Lorant, A., et al. (2019). Migratory DCs activate TGF-beta to precondition naive $CD8^+$ T cells for tissue-resident memory fate. Science *366*, eaav5728. https://doi.org/10.1126/science.aav5728.
60. Cerutti, A., and Rescigno, M. (2008). The biology of intestinal immunoglobulin A responses. Immunity *28*, 740–750. https://doi.org/10.1016/j.immuni.2008.05.001.
61. Hall, J.A., Cannons, J.L., Grainger, J.R., Dos Santos, L.M., Hand, T.W., Naik, S., Wohlfert, E.A., Chou, D.B., Oldenhove, G., Robinson, M., et al. (2011). Essential role for retinoic acid in the promotion of CD4(+) T cell effector responses via retinoic acid receptor alpha. Immunity *34*, 435–447. https://doi.org/10.1016/j.immuni.2011.03.003.
62. Mohammed, J., Beura, L.K., Bobr, A., Astry, B., Chicoine, B., Kashem, S.W., Welty, N.E., Igyártó, B.Z., Wijeyesinghe, S., Thompson, E.A., et al. (2016). Stromal cells control the epithelial residence of DCs and memory T cells by regulated activation of TGF-β. Nat. Immunol. *17*, 414–421. https://doi.org/10.1038/ni.3396.
63. Evrard, M., Becht, E., Fonseca, R., Obers, A., Park, S.L., Ghabdan-Zanluqui, N., Schroeder, J., Christo, S.N., Schienstock, D., Lai, J., et al. (2023). Single-cell protein expression profiling resolves circulating and resident memory T cell diversity across tissues and infection contexts. Immunity *56*, 1664–1680.e9. https://doi.org/10.1016/j.immuni.2023.06.005.
64. von Hoesslin, M., Kuhlmann, M., de Almeida, G.P., Kanev, K., Wurmser, C., Gerullis, A.K., Roelli, P., Berner, J., and Zehn, D. (2022). Secondary infections rejuvenate the intestinal $CD103^+$ tissue-resident memory T cell pool. Sci. Immunol. *7*, eabp9553. https://doi.org/10.1126/sciimmunol.abp9553.
65. Fung, H.Y., Teryek, M., Lemenze, A.D., and Bergsbaken, T. (2022). CD103 fate mapping reveals that intestinal $CD103^-$ tissue-resident memory T cells are the primary responders to secondary infection. Sci. Immunol. *7*, eabl9925. https://doi.org/10.1126/sciimmunol.abl9925.
66. Restori, K.H., McDaniel, K.L., Wray, A.E., Cantorna, M.T., and Ross, A.C. (2014). Streptococcus pneumoniae-induced pneumonia and Citrobacter rodentium-induced gut infection differentially alter vitamin A concentrations in the lung and liver of mice. J. Nutr. *144*, 392–398. https://doi.org/10.3945/jn.113.186569.
67. Hurst, R.J., and Else, K.J. (2013). The retinoic acid-producing capacity of gut dendritic cells and macrophages is reduced during persistent T. muris infection. Parasite Immunol. *35*, 229–233. https://doi.org/10.1111/pim.12032.
68. Grizotte-Lake, M., Zhong, G., Duncan, K., Kirkwood, J., Iyer, N., Smolenski, I., Isoherranen, N., and Vaishnava, S. (2018). Commensals Suppress Intestinal Epithelial Cell Retinoic Acid Synthesis to Regulate Interleukin-22 Activity and Prevent Microbial Dysbiosis. Immunity *49*, 1103–1115.e6. https://doi.org/10.1016/j.immuni.2018.11.018.
69. World Health Organization (2009). Global prevalence of vitamin A deficiency in populations at risk 1995-2005: WHO global database on vitamin A deficiency. https://www.who.int/publications/i/item/9789241598019.
70. Stephensen, C.B. (2001). Vitamin A, infection, and immune function. Annu. Rev. Nutr. *21*, 167–192. https://doi.org/10.1146/annurev.nutr.21.1.167.
71. Park, S.L., Zaid, A., Hor, J.L., Christo, S.N., Prier, J.E., Davies, B., Alexandre, Y.O., Gregory, J.L., Russell, T.A., Gebhardt, T., et al. (2018). Local proliferation maintains a stable pool of tissue-resident memory T cells after antiviral recall responses. Nat. Immunol. *19*, 183–191. https://doi.org/10.1038/s41590-017-0027-5.
72. Davies, B., Prier, J.E., Jones, C.M., Gebhardt, T., Carbone, F.R., and Mackay, L.K. (2017). Cutting Edge: Tissue-Resident Memory T Cells Generated by Multiple Immunizations or Localized Deposition Provide Enhanced Immunity. J. Immunol. *198*, 2233–2237. https://doi.org/10.4049/jimmunol.1601367.
73. Di Marco Barros, R., Roberts, N.A., Dart, R.J., Vantourout, P., Jandke, A., Nussbaumer, O., Deban, L., Cipolat, S., Hart, R., Iannitto, M.L., et al. (2016). Epithelia Use Butyrophilin-like Molecules to Shape Organ-Specific γδ T Cell Compartments. Cell *167*, 203–218.e17. https://doi.org/10.1016/j.cell.2016.08.030.
74. Bandeira, A., Mota-Santos, T., Itohara, S., Degermann, S., Heusser, C., Tonegawa, S., and Coutinho, A. (1990). Localization of gamma/delta T cells to the intestinal epithelium is independent of normal microbial colonization. J. Exp. Med. *172*, 239–244. https://doi.org/10.1084/jem.172.1.239.
75. Park, S.L., Christo, S.N., Wells, A.C., Gandolfo, L.C., Zaid, A., Alexandre, Y.O., Burn, T.N., Schröder, J., Collins, N., Han, S.J., et al. (2023). Divergent molecular networks program functionally distinct $CD8^+$ skin-resident memory T cells. Science *382*, 1073–1079. https://doi.org/10.1126/science.adi8885.
76. Cheng, Y., Wong, M.T., van der Maaten, L., and Newell, E.W. (2016). Categorical Analysis of Human T Cell Heterogeneity with One-Dimensional Soli-Expression by Nonlinear Stochastic Embedding. J Immunol *196*, 924–932. https://doi.org/10.4049/jimmunol.1501928.
77. Kolde, R. (2019). pheatmap: Pretty Heatmaps. R package version 1.0.12. https://CRAN.R-project.org/package=pheatmap.
78. Conway J. (2019). UpSetR: A More Scalable Alternative to Venn and Euler Diagrams for Visualizing Intersecting Sets. R package version 1.4.0. https://cran.r-project.org/package=UpSetR.
79. Melville, J., Lun, A., Djekidel, M.N., Hao, Y., and Eddelbuettel, D. (2022). uwot: The Uniform Manifold Approximation and Projection (UMAP) Method for Dimensionality Reduction. R package version 0.1.14. https://CRAN.R-project.org/package=uwot.
80. Ritchie, M.E., Phipson, B., Wu, D., Hu, Y., Law, C.W., Shi, W., and Smyth, G.K. (2015). limma powers differential expression analyses for RNA-sequencing and microarray studies. Nucleic Acids Res. *43*, e47. https://doi.org/10.1093/nar/gkv007.
81. Chen, Y., Chen, L., Lun, A.T.L., Baldoni, P.L., and Smyth, G.K. (2024). edgeR 4.0: powerful differential analysis of sequencing data with expanded functionality and improved support for small counts and larger datasets. bioRxiv. https://doi.org/10.1101/2024.01.21.576131.
82. Risso, D., Ngai, J., Speed, T.P., and Dudoit, S. (2014). Normalization of RNA-seq data using factor analysis of control genes or samples. Nat Biotechnol *32*, 896–902. https://doi.org/10.1038/nbt.2931.
83. Kallert, S.M., Darbre, S., Bonilla, W.V., Kreutzfeldt, M., Page, N., Müller, P., Kreuzaler, M., Lu, M., Favre, S., Kreppel, F., et al. (2017). Replicating viral vector platform exploits alarmin signals for potent $CD8^+$ T cell-mediated tumour immunotherapy. Nat. Commun. *8*, 15327. https://doi.org/10.1038/ncomms15327.
84. Cheng, Y., Wong, M.T., van der Maaten, L., and Newell, E.W. (2016). Categorical Analysis of Human T Cell Heterogeneity with One-Dimensional Soli-Expression by Nonlinear Stochastic Embedding. J. Immunol. *196*, 924–932. https://doi.org/10.4049/jimmunol.1501928.

85. Corces, M.R., Buenrostro, J.D., Wu, B., Greenside, P.G., Chan, S.M., Koenig, J.L., Snyder, M.P., Pritchard, J.K., Kundaje, A., Greenleaf, W.J., et al. (2016). Lineage-specific and single-cell chromatin accessibility charts human hematopoiesis and leukemia evolution. Nat. Genet. *48*, 1193–1203. https://doi.org/10.1038/ng.3646.

86. Dominguez, C.X., Amezquita, R.A., Guan, T., Marshall, H.D., Joshi, N.S., Kleinstein, S.H., and Kaech, S.M. (2015). The transcription factors ZEB2 and T-bet cooperate to program cytotoxic T cell terminal differentiation in response to LCMV viral infection. J. Exp. Med. *212*, 2041–2056. https://doi.org/10.1084/jem.20150186.

87. Tsyganov, K., James Perry, A., Kenneth Archer, S., and Powell, D. (2018). RNAsik: A Pipeline for complete and reproducible RNA-seq analysis that runs anywhere with speed and ease. J. Open Source Software *3*, 3. https://doi.org/10.21105/joss.00583.

88. Fonseca, R., Burn, T.N., Gandolfo, L.C., Devi, S., Park, S.L., Obers, A., Evrard, M., Christo, S.N., Buquicchio, F.A., Lareau, C.A., et al. (2022). Runx3 drives a $CD8^+$ T cell tissue residency program that is absent in $CD4^+$ T cells. Nat. Immunol. *23*, 1236–1245. https://doi.org/10.1038/s41590-022-01273-4.

89. Robinson, M.D., and Oshlack, A. (2010). A scaling normalization method for differential expression analysis of RNA-seq data. Genome Biol. *11*, R25. https://doi.org/10.1186/gb-2010-11-3-r25.

90. Molania, R., Gagnon-Bartsch, J.A., Dobrovic, A., and Speed, T.P. (2019). A new normalization for Nanostring nCounter gene expression data. Nucleic Acids Res. *47*, 6073–6083. https://doi.org/10.1093/nar/gkz433.

91. Gandolfo, L.C., and Speed, T.P. (2018). RLE plots: Visualizing unwanted variation in high dimensional data. PLoS One *13*, e0191629. https://doi.org/10.1371/journal.pone.0191629.

92. Risso, D., Schwartz, K., Sherlock, G., and Dudoit, S. (2011). GC-content normalization for RNA-Seq data. BMC Bioinformatics *12*, 480. https://doi.org/10.1186/1471-2105-12-480.

93. Leek, J.T. (2014). svaseq: removing batch effects and other unwanted noise from sequencing data. Nucleic Acids Res. *42*, e161. https://doi.org/10.1093/nar/gku864.

STAR★METHODS

KEY RESOURCES TABLE

REAGENT or RESOURCE	SOURCE	IDENTIFIER
Antibodies		
Anti-B220 (clone RA3-6B2; BUV395)	BD Biosciences	Cat#563793; RRID: AB_2738427
Anti-B220 (clone RA3-6B2; BV750)	Biolegend	Cat#103261; RRID: AB_2734157
Anti-Bcl2 (clone 3F11; PE)	BD Biosciences	Cat#556537; RRID: AB_396457
anti-Bim (clone C34C5; AF488)	Cell Signaling	Cat#94805; RRID: AB_2800234
Anti-CD8α (clone 53-6.7; BV711)	BD Biosciences	Cat#563046; RRID: AB_2737972
Anti-CD8α (clone 53-6.7; SparkNIR685)	Biolegend	Cat#100782; RRID: AB_2819775
Anti-CD8β (clone H35-17.2; BV750)	BD Biosciences	Cat#747505; RRID: AB_2872172
Anti-CD8β (clone H35-17.2; BV786)	BD Biosciences	Cat#740952; RRID: AB_2740577
Anti-CD11a (clone M17/4; BB700)	BD Biosciences	Cat#742109; RRID: AB_2871382
Anti-CD11b (clone M1/70; BUV661)	BD Biosciences	Cat#612977; RRID: AB_2870249
Anti-CD18 (clone C71/16; BV750)	BD Biosciences	Cat#747153; RRID: AB_2871894
Anti-CD38 (clone 90; BV750)	BD Biosciences	Cat#747103; RRID: AB_2871855
Anti-CD38 (clone 90; APC/Fire810)	Biolegend	Cat#102746; RRID: AB_2890674
Anti-CD39 (clone Y23-1185; BV711)	BD Biosciences	Cat#567295; RRID: AB_2916538
Anti-CD43 (clone S11; FITC)	Biolegend	Cat#143204; RRID: AB_10960745
Anti-CD44 (clone IM7; BUV395)	BD Biosciences	Cat#740215; RRID: AB_2739963
Anti-CD44 (clone IM7; BV510)	BD Biosciences	Cat#563114; RRID: AB_2738011
Anti-CD44 (clone IM7; APC/R700)	BD Biosciences	Cat#565480; RRID: AB_2739259
Anti-CD45.1 (clone A20; BV480)	BD Biosciences	Cat#746666; RRID: AB_2743938
Anti-CD45.1 (clone A20; PE/Cy7)	Biolegend	Cat#110730; RRID: AB_1134168
Anti-CD45.1 (clone A20; APC/R700)	BD Biosciences	Cat#565814; RRID: AB_2744397
Anti-CD45.2 (clone 104; APC)	Biolegend	Cat#109814; RRID: AB_389211
Anti-CD45.2 (clone 104; SparkNIR685)	Biolegend	Cat#109864; RRID: AB_2876424
Anti-CD45RB (clone 16A; BUV395)	BD Biosciences	Cat#740211; RRID: AB_2739959
Anti-CD49a (clone Ha31/8; BV510)	BD Biosciences	Cat#740144; RRID: AB_2739900
Anti-CD49a (clone Ha31/8; BV605)	BD Biosciences	Cat#740375; RRID: AB_2740107
Anti-CD49a (clone Ha31/8; BV711)	BD Biosciences	Cat#564863; RRID: AB_2738987
Anti-CD55 (clone RIKO-3; PE/Cy7)	Biolegend	Cat#131814; RRID: AB_2800634
Anti-CD55 (clone RIKO-3; APC)	Biolegend	Cat#131812; RRID: AB_2800632
Anti-CD62L (clone MEL-14; BUV737)	BD Biosciences	Cat#612833; RRID: AB_2870155
Anti-CD62L (clone MEL-14; BV605)	BD Biosciences	Cat#563252; RRID: AB_2738098
Anti-CD62L (clone MEL-14; APC/R700)	BD Biosciences	Cat#565159; RRID: AB_2737397
Anti-CD69 (clone H1.2F3; PE/Cy5)	Biolegend	Cat#104510; RRID: AB_313113
Anti-CD69 (clone H1.2F3; SparkNIR685)	Biolegend	Cat#104558; RRID: AB_2876411
Anti-CD73 (clone TY/11.8; BV421)	Biolegend	Cat#127217; AB_2687251
Anti-CD73 (clone TY/11.8; eF450)	Thermo Fisher Scientific	Cat#48-0731-82; RRID: AB_1272196
Anti-CD101 (clone Moushi101; PE)	Thermo Fisher Scientific	Cat#12-1011-82; RRID: AB_1210728
Anti-CD101 (clone Moushi101; PE/Cy7)	Thermo Fisher Scientific	Cat#25-1011-82; RRID: AB_2573378
Anti-CD103 (clone 2E7; eF450)	Thermo Fisher Scientific	Cat#48-1031-82; RRID: AB_2574033
Anti-CD103 (clone M290; BV480)	BD Biosciences	Cat#566118; RRID: AB_2739520
Anti-CD122 (clone 5H4; PE)	Biolegend	Cat#105906; RRID: AB_2125736
Anti-CD127 (clone A7R34; PE/eF610)	Thermo Fisher Scientific	Cat#61-1271-82; RRID: AB_2802381
Anti-Collagen IV (rabbit polyclonal)	Abcam	Cat#ab19808; RRID: AB_445160
Anti-CXCR3 (clone CXCR3-173; BV605)	Biolegend	Cat#155915; RRID: AB_2892317

(*Continued on next page*)

Continued

REAGENT or RESOURCE	SOURCE	IDENTIFIER
Anti-CXCR3 (clone CXCR3-173; BV650)	Biolegend	Cat#126531; RRID: AB_2563160
Anti-CXCR6 (clone SA051D1; BV421)	Biolegend	Cat#151109; RRID: AB_2616760
Anti-CXCR6 (clone SA051D1; PE)	Biolegend	Cat#151104; RRID: AB_2566546
Anti-CXCR6 (clone SA051D1; PE/Dazzle594)	Biolegend	Cat#151117; RRID: AB_2721700
Anti-CXCR6 (clone SA051D1; APC)	Biolegend	Cat#151106; RRID: AB_2572143
Anti-CX3CR1 (clone SA011F11; BV421)	Biolegend	Cat#149023; RRID: AB_2565706
Anti-CX3CR1 (clone SA011F11; BV711)	Biolegend	Cat#149031; RRID: AB_2565939
Anti-CX3CR1 (clone SA011F11; BV785)	Biolegend	Cat#149029; RRID: AB_2565938
Anti-CX3CR1 (clone SA011F11; PE/Dazzle594)	Biolegend	Cat#149014; RRID: AB_2565698
Anti-CX3CR1 (clone SA011F11; APC)	Biolegend	Cat#149008; RRID: AB_2564492
Anti-Eomes (clone Dan11mag; PE/Cy7)	Thermo Fisher Scientific	Cat#25-4875-82; RRID: AB_2573454
Anti-EpCAM (clone G8.8; Biotin)	Biolegend	Cat#118204; RRID: AB_1134178
anti-FoxP3 (clone FJK-16s; eF450)	Thermo Fisher Scientific	Cat#25-4875-82; RRID: AB_1518812
anti-GATA3 (clone L50-823; PE/Cy7)	BD Biosciences	Cat#560405; RRID: AB_1645544
Anti-Granzyme A (clone GzA-3G8.5; eF450)	Thermo Fisher Scientific	Cat#48-5831-82; RRID: AB_2574079
Anti-Granzyme B (clone QA16A02; FITC)	Biolegend	Cat#372206; RRID: AB_2687030
Anti-Granzyme B (clone QA16A02; AF700)	Biolegend	Cat#372222; RRID: AB_2728389
Anti-IFNγ (clone XMG1.2; BV480)	BD Biosciences	Cat#566097; RRID: AB_2739501
Anti-IFNγ (clone XMG1.2; FITC)	BD Biosciences	Cat#554411; RRID: AB_395375
Anti-IL-2 (clone JES6-5H4; PE)	Biolegend	Cat#503808; RRID: AB_315302
Anti-IL-2 (clone JES6-5H4; APC)	Biolegend	Cat#503810; RRID: AB_315304
Anti-IL18Ra (clone P3TUNYA; eF450)	Thermo Fisher Scientific	Cat#48-5183-82; RRID: AB_2574069
Anti-Integrinβ7 (clone M293; BV650)	BD Biosciences	Cat#743790; RRID: AB_2741758
Anti-Ki67 (clone SolA15; FITC)	Thermo Fisher Scientific	Cat#11-5698-82; RRID: AB_11151330
Anti-Ki67 (clone SolA15; APC/eF780)	Thermo Fisher Scientific	Cat#47-5698-82; RRID: AB_2688065
Anti-KLRG1 (clone 2F1; BV421)	BD Biosciences	Cat#562897; RRID: AB_2737875
Anti-KLRG1 (clone 2F1; PE/eF610)	Thermo Fisher Scientific	Cat#61-5893-82; RRID: AB_2574630
Anti-KLRG1 (clone 2F1; APC/eF780)	Thermo Fisher Scientific	Cat#47-5893-82; RRID: AB_2573988
Anti-Ly6A/E (clone D7; BUV805)	BD Biosciences	Cat#741916; RRID: AB_2871229
Anti-Ly6C (clone HK1.4; BV570)	Biolegend	Cat#128030; RRID: AB_2562617
Anti-Ly6C (clone HK1.4; BV605)	Biolegend	Cat#128036; RRID: AB_2562353
Anti-Ly6C (clone HK1.4; BV785)	Biolegend	Cat#128041; RRID: AB_2565852
Anti-LyVE1 (clone ALY7; eF570)	Thermo Fisher Scientific	Cat#41-0443-82; RRID: AB_2573596
Anti-MHCII (clone M5/114.15.2; SparkBlue550)	Biolegend	Cat#107662; RRID: AB_2860616
Anti-NK1.1 (clone PK136; BUV563)	BD Biosciences	Cat#741233; RRID: AB_741233
Anti-NK1.1 (clone PK136; BV480)	BD Biosciences	Cat#746265; RRID: AB_2743597
Anti-NK1.1 (clone PK136; SparkNIR685)	Biolegend	Cat#156529; RRID: AB_2910321
Anti-NKG2D (clone CX5; PE/eF610)	Thermo Fisher Scientific	Cat# 61-5882-82; RRID: AB_2574628
Anti-PD1 (clone 29F.1A12; BV711)	Biolegend	Cat#135231; RRID: AB_2566158
Anti-PD1 (clone 29F.1A12; BV785)	Biolegend	Cat#329930; RRID: AB_2563443
Anti-PD1 (clone 29F.1A12; PE/Fire810)	Biolegend	Cat#135253; RRID: AB_2910293
anti-RORγt (clone Q31-378, BV421)	BD Biosciences	Cat#562894; RRID: AB_2687545
Anti-Runx3 (clone R3-5G4; PE)	BD Biosciences	Cat#564814; RRID: AB_2738969
Anti-Tbet (clone 4B10; BV421)	Biolegend	Cat#644815; RRID: AB_10896427
Anti-Tbet (clone 4B10; AF488)	Biolegend	Cat#644830; RRID: AB_2566019
Anti-Tbet (clone 4B10; PE)	Biolegend	Cat#644810; RRID: AB_2200542

(*Continued on next page*)

Continued

REAGENT or RESOURCE	SOURCE	IDENTIFIER
Anti-TCF1 (clone C63D9; AF488)	Cell Signaling	Cat#2203S; RRID: AB_2199302
Anti-TCRβ (clone H57-597; BV650)	Biolegend	Cat#109251; RRID: AB_2810348
Anti-TCRβ (clone H57-597; BV711)	Biolegend	Cat#109243; RRID: AB_2629564
Anti-TCRβ (clone H57-597; APC/Fire750)	Biolegend	Cat#109246; RRID: AB_2629697
Anti-TCRγδ (clone GL3; BV605)	Biolegend	Cat#118129; RRID: AB_2563356
Anti-TCRγδ (clone GL3; PerCP/eF710)	Thermo Fisher Scientific	Cat#46-5711-82; RRID: AB_2016707
Anti-TCRγδ (clone GL3; RB780)	BD Biosciences	Cat# 755465; RRID: N/A
Anti-Thy1.1 (clone OX-7; AF488)	Biolegend	Cat#202506; RRID: AB_492882
Anti-Thy1.1 (clone OX-7; PerCP)	Biolegend	Cat#202512; RRID: AB_1595487
Anti-Thy1.1 (clone OX7; AF647)	Biolegend	Cat#202508; RRID: AB_492884
Anti-Thy1.1 (clone OX-7; AF700)	Biolegend	Cat#202528; RRID: AB_1626241
Anti-Thy1.2 (clone 53-2.1; BUV395)	BD Biosciences	Cat#565257; RRID: AB_2739136
Anti-Thy1.2 (clone 53-2.1; PerCP)	Biolegend	Cat#140316; RRID: AB_10642813
Anti-TNF (clone MP6-XT22; BV711)	Biolegend	Cat#506349; RRID: AB_2629800
Anti-Vα2 (clone B20.1; BUV615)	BD Biosciences	Cat#751416; RRID: AB_2875415
Anti-Vα2 (clone B20.1; BV421)	BD Biosciences	Cat#562944; RRID: AB_2737910
Anti-Vα2 (clone B20.1; BV480)	BD Biosciences	Cat#746615; RRID: AB_2743895
Anti-Vα2 (clone B20.1; PE)	BD Biosciences	Cat#553289; RRID: AB_394760
Anti-Vα2 (clone B20.1; PE/Cy7)	BD Biosciences	Cat#560624; RRID: AB_1727584
Goat anti-Rabbit IgG AF405	Thermo Fisher Scientific	Cat#A-31556; RRID: AB_221605
Streptavidin DyLight800	Thermo Fisher Scientific	Cat#21851; RRID: N/A
Anti-Ter119 (clone Ter119; purified from hybridoma)	In house	N/A
Anti-MHCII (clone M5/114.15.2 purified from hybridoma)	In house	N/A
Anti-CD4 (clone GK1.5; purified from hybridoma)	In house	N/A
Anti-CD11b (clone: M1/70; purified from hybridoma	In house	N/A
Anti-F4/80 (clone BM8; purified from hybridoma)	In house	N/A
Anti-Thy1 (clone T24; purified from hybridoma)	In house	N/A
Anti-CD3 (clone 145-2C11)	BioXCell	Cat#BE0001-1; RRID: AB_1107634
Anti-CD28 (clone 37.51)	BioXCell	Cat#BE0015-1; RRID: AB_1107624
Anti-ARTC2 (Treg protector) (clone S+16a)	Biolegend	Cat#149802; RRID: AB_2565494
Bacterial and virus strains		
Herpes simplex virus (HSV-OVA)	D. Tscharke, Australian National University	N/A
Lymphocytic choriomeningitis virus (LCMV) Armstrong strain	R. Ahmed, Emory University	N/A
Lymphocytic choriomeningitis virus (LCMV)-OVA	D. Merkler, University of Geneva	N/A
Listeria monocytogenes (Lm-OVA), InlA mutant	L. Lefrancois, University of Connecticut	N/A
Chemicals, peptides, and recombinant proteins		
GP33 peptide (KAVYNFATM)	Auspep	N/A
OVA peptide (SIINFEKL)	Auspep	N/A
Alt-R S.p. Cas9 Nuclease V3	Integrated DNA Technologies	Cat#1081059
Collagenase type III	Worthington Biochemical	Cat#LS004183

(*Continued on next page*)

Continued

REAGENT or RESOURCE	SOURCE	IDENTIFIER
Dispase II (neutral protease, grade II)	Roche	Cat#4942078001
Deoxyribonuclease I from bovine pancreas	Sigma-Aldrich	Cat#DN25
Percoll	Thermo Fisher Scientific	Cat#GE17-0891-01
1,4-Dithioerythritol (DTE)	Sigma-Aldrich	Cat#D8255
10X HBSS, no Ca^{2+}, no Mg^{2+}	Thermo Fisher Scientific	Cat#14180046
eBioscience 1X RBC Lysis Buffer	Thermo Fisher Scientific	Cat#00-4333-57
Brefeldin A from Penicillium	Sigma-Aldrich	Cat#B6542
Retinoic acid	Sigma-Aldrich	Cat#R2625
Human recombinant TGF-β1 (carrier-free)	Biolegend	Cat#781804
Human recombinant IL-2	Peprotech	Cat#200-02
Human recombinant IL-15	Biolegend	Cat#570314
Murine recombinant IL-15	Peprotech	Cat#210-15
EDTA	Sigma-Aldrich	Cat#E5134
Trypsin-EDTA Solution 10X	Sigma-Aldrich	Cat#59418C
LPS from *E.coli* O111:B4	Sigma-Aldrich	Cat#L4391
Bovine serum albumin	Sigma-Aldrich	Cat#A7906
Fetal Bovine serum	Sigma-Aldrich	Cat#12007C
Penicillin/Streptomycin	Sigma-Aldrich	Cat#P0781
2-Mercaptoethanol	Sigma-Aldrich	Cat#M3148
L-Glutamine	Sigma-Aldrich	Cat# G8540
DMEM	In house	N/A
RPMI	In house	N/A
HEPES	Sigma-Aldrich	Cat#H3375
BioMag Goat Anti-Rat IgG	Qiagen	Cat#310107
EasySep Mouse Naïve CD8+ T Cell Isolation Kit	StemCell Technologies	Cat#19858
Sphero blank calibration particles	BD Bioscience	Cat#556296
Acetone	Sigma-Aldrich	Cat#179124
1-Fluoro-2,4-dinitrobenzene (DNFB)	Sigma-Aldrich	Cat#D1529
AGN194310 (RA antagonist)	Sigma-Aldrich	Cat#SML2665
AM80 (RA agonist)	Sigma-Aldrich	Cat#T3205
Fingolimod (FTY720)	Sapphire Bioscience	Cat#10006292
(2-Hydroxypropyl)-β-cyclodextrin	Sigma-Aldrich	Cat#C0926
Pierce 16% Formaldehyde (w/v), Methanol-free	Thermo Fisher Scientific	Cat#28908
Tissue-Tek O.C.T. Compound	Sakura Finetek	Cat#4583
ProLong Diamond Antifade Mountant	Thermo Fisher Scientific	Cat#P36965
DAPI (4',6-Diamidino-2-Phenylindole, Dilactate)	Biolegend	Cat#422801
Critical commercial assays		
Zombie Yellow Fixable Viability Kit	Biolegend	Cat#423104
Zombie NIR Fixable Viability Kit	Biolegend	Cat#423106
RNeasy Plus Micro Kit	Qiagen	Cat#74034
P3 Primary Cell 4D-NucleofectorTM X Kit S	Lonza	Cat#V4XP-3032
BD Cytofix/Cytoperm Fixation/ Permeabilization Kit	BD Bioscience	Cat#554714; RRID: AB_2869008
eBioscience FoxP3/Transcription Factor Staining Buffer Set	Thermo Fisher Scientific	Cat#00-5523-00
High-Capacity cDNA Reverse Transcription Kit	Thermo Fisher Scientific	Cat# 4368814

(*Continued on next page*)

Continued

REAGENT or RESOURCE	SOURCE	IDENTIFIER
TruSeq Stranded mRNA Library Prep	Illumina	Cat#20020594
SMART-Seq HT PLUS Kit	Takara	Cat#R400749
Deposited data		
GEO: GSE232852 (RNA-seq *in vitro* $CD8^+$ T cells)	This paper	https://www.ncbi.nlm.nih.gov/geo/query/acc.cgi?acc=GSE232852
GEO: (RNA-seq dnRARα-RV)	This paper	https://www.ncbi.nlm.nih.gov/geo/query/acc.cgi?acc=GSE277247
GEO: GSE277248 (RNA-seq RA antag.)	This paper	https://www.ncbi.nlm.nih.gov/geo/query/acc.cgi?acc=GSE277248
GEO: GSE277120 (ATAC-seq *Tbx21*$^{-/-}$ $CD8^+$ T cells)	This paper	https://www.ncbi.nlm.nih.gov/geo/query/acc.cgi?acc=GSE277120
BioProject: PRJNA1153786	This paper	https://www.ncbi.nlm.nih.gov/bioproject/?term=PRJNA1153786
Experimental models: Cell lines		
Platinum-E (Plat-E) cell line	Cell Biolabs, Inc.	Cat#RV-101; RRID: CVCL_B488
Experimental models: Organisms/strains		
Mouse: C57BL/6J	The Jackson Laboratory	Strain #:000664; RRID: IMSR_JAX:000664
Mouse: B6;D2-Tg(TcrLCMV)327Sdz/JDvsJ (P14)	The Jackson Laboratory	Strain #:004694; RRID:IMSR_JAX:004694
Mouse: C57BL/6-Tg(TcraTcrb)1100Mjb/J (OT-I)	The Jackson Laboratory	Strain #:003831; RRID:IMSR_JAX:003831
Mouse: B6.SJL-*Ptprc*^{a} *Pepc*^{b}/BoyJ (CD45.1)	The Jackson Laboratory	Strain #:002014; RRID:IMSR_JAX:002014
Mouse: B6.PL-*Thy1*^{a}/CyJ (Thy1.1)	The Jackson Laboratory	Strain #:000406; RRID:IMSR_JAX:000406
Mouse: B6;129-*Tgfbr2*^{tm1Karl}/J (*Tgfbr2*$^{fl/fl}$)	The Jackson Laboratory	Strain #:012603;RRID:IMSR_JAX:012603
Mouse: B6.Cg-Tg(Lck-icre)3779Nik/J (dLck^{cre})	The Jackson Laboratory	Strain #:012837; RRID:IMSR_JAX:012837
Mouse: Zfp683-TdTomato (Hobit^{Tom})	N/A	N/A
Mouse: B6.129X1-*Gt(ROSA)26Sor*$^{tm1(EYFP)Cos}$/J (R26R-YFP)	The Jackson Laboratory	Strain #:006148; RRID:IMSR_JAX:006148
Mouse: JaCa (James Cagney) wild	This paper	N/A
Oligonucleotides		
Hic1 sgRNA#1: AGUGUGCGGAAAGCGCGGAG	Synthego	N/A
Hic1 sgRNA#2: CUUGUGCGACGUGAUCAUCG	Synthego	N/A
Itgae sgRNA#1: GUCAUGGUGGUACUUACUGA	Synthego	N/A
Itgae sgRNA#2: GAUUGCCUCAGACCCCAAAG	Synthego	N/A
P2rx7 sgRNA#1: UGAGCGAUAAGCUGUACCAG	Synthego	N/A
P2rx7 sgRNA#2: UAUCAGCUCCGUGCACACCA	Synthego	N/A
Tbx21 sgRNA#1: UGAACUUGGACCACAACAGG	Synthego	N/A
Tbx21 sgRNA#2: GCGGUACCAGAGCGGCAAGU	Synthego	N/A
Cd19 sgRNA#1: AAUGUCUCAGACCAUAUGGG	Synthego	N/A
Cd19 sgRNA#1: GAGAAGCUGGCUUGGUAUCG	Synthego	N/A

(*Continued on next page*)

Continued

REAGENT or RESOURCE	SOURCE	IDENTIFIER
Recombinant DNA		
pCL-Eco retrovirus packaging vector	Addgene	RRID: Addgene_12371
pMSCV-IRES-GFP II (pMIG II) vector	Addgene	RRID: Addgene_52107
pMIG II dnRARα vector	This paper	N/A
pMSCV-IRES-mAmetrine 1.1 FP (pMIA) vector	Addgene	RRID: Addgene_52113
pMIA CCR9 vector	This paper	N/A
Software and algorithms		
FlowJo v10	Tree Star	https://www.flowjo.com/
Prism v10	GraphPad	https://www.graphpad.com/
OMIQ	Dotmatics	https://www.omiq.ai/
oneSENSE v1.20	Cheng[76]	https://bioconductor.org/packages/oneSENSE/
pheatmap v1.0.12	Kolde[77]	https://cran.r-project.org/package=pheatmap
UpSetR v1.4.0	Conway[78]	https://cran.r-project.org/web/packages/UpSetR/index.html
uwot v0.1.14	Melville[79]	https://cran.r-project.org/package=uwot
limma v3.60.4	Richie[80]	https://www.bioconductor.org/packages/release/bioc/html/limma.html
edgeR v4.2.1	Chen[81]	https://www.bioconductor.org/packages/release/bioc/html/edgeR.html
RUVseq v1.38.0	Risso[82]	https://www.bioconductor.org/packages/release/bioc/html/RUVSeq.html

EXPERIMENTAL MODEL AND SUBJECT DETAILS

Mice

C57BL/6, B6.SJL-PtprcaPep3b/BoyJ (CD45.1), B6.SJL-PtprcaPep3b/BoyJ × C57BL/6 (CD45.1×CD45.2), P14 CD45.1, P14 *Zfp683*$^{\text{cre-tdTomato/+}}$ × R26R-EYFP (P14 *Hobit*$^{\text{cre-tdTomato}}$:*Rosa26*$^{\text{LsL-YFP}}$), OT-I CD45.1, OT-I *Tbx21*$^{-/-}$, OT-I *Tgfbr2*$^{f/f}$.dLck-cre CD45.1 (OT-I *Tgfbr2*$^{-/-}$), OT-I *Tbx21*$^{-/-}$*Tgfbr2*$^{-/-}$, *Il15*$^{-/-}$, and *Hic1*$^{\text{Citrine/+}}$ mice were bred in the Department of Microbiology and Immunology. *Zfp683*$^{\text{cre-tdTomato/+}}$ mice were generated by the Kallies lab and will be described in detail elsewhere. Female mice were used for experiments at 6-20 weeks of age. P14 mice express a transgenic T cell receptor recognizing the LCMV glycoprotein-derived epitope GP_{33-41}. OT-I mice express a transgenic T cell receptor recognizing the ovalbumin epitope $OVA_{257-264}$. James Cagney (JaCa) 'dirty' mice were generated by Tri Giang Phan (Garvan Institute of Medical Research) and Jenny Kingham (Australian BioResources) with approval from the Garvan/St Vincent's Animal Ethics Committee (#17_16 and 20_19). Briefly, outbred wildtype mice were sourced from a public educational farm (Calmsley Hill City Farm). To establish breeding pairs for the JaCa colony, mice were sprayed with a topical application of Ivermectin (1g/ml) and 24 hours later were on continuous treatment with Fenbendazole (150ppm) medicated feed to treat pinworms. Sentinel mice were screened by serology every six months for Mouse hepatitis virus, Mouse parvovirus, Minute virus of mice, Mouse norovirus, Theiler's encephalomyelitis virus and Rotavirus, and PCR on pooled faeces to detect *Helicobacter spp*. fecal pellets were collected and stored at -80°C and processed in batches. 16s rRNA sequencing was performed to ensure the diversity and stability of the vertically transmitted microbiota was maintained in the offsprings. For co-housing experiments, JaCa female mice were cohoused with >12-weeks old female C57BL/6 for >30 days for horizontal transmission of the microbiota. Age- and sex-matched C57BL/6 were maintained under SPF conditions. All animal experiments were approved by the University of Melbourne Animal Ethics Committee.

T cell transfer

For adoptive transfers of naive P14 or OT-I cells were carried out intravenously (i.v.) with lymph node suspensions. Naive P14 or OT-I cells were transferred at a total number of 5×10^4 or 2.5×10^4 cells/population in co-transfer experiments, where cell types were transferred at a ratio of 1:1. For in vitro-activated T cell transfer, P14 or OT-I cells were activated in culture for 4–5 d with GP_{33-41} (KAVYNFATM) or $OVA_{257-264}$ (SIINFEKL) peptide-pulsed splenocytes, respectively, in the presence of recombinant human IL-2 (25 U/mL; PeproTech), or with atRA (10 nM, Sigma Aldrich) at 37°C and 5% CO_2. Cells were transferred i.v. to naïve recipient mice at a total of $3.5\text{-}10\times10^6$ cells/population.

Infections and DNFB treatment

HSV infection was performed by scarification using 1×10^6 plaque forming units (pfu) of the KOS strain of the virus modified to express ovalbumin protein (HSV-OVA).[11] LCMV-OVA (artLCMV) was obtained from Doron Merkler.[83] LCMV infection was performed by intraperitoneal (i.p.) injection of 2×10^5 pfu of the Armstrong strain of LCMV or 10^5 pfu of the OVA strain of LCMV. Lm infection was performed through oral feeding using a recombinant strain that carries OVA and a mutated internalin A. Mice were infected with 10^9 cfu of Lm-OVA as described.[26] For DNFB treatment, mice were shaved and depilated before application of 15-20 μL of DNFB (0.25%) in acetone and oil (4:1) to a 1.5cm^2 region of skin on the same day as activated T cell transfer or 3 days following LCMV infection.

In vivo treatments

Mice were injected intraperitoneally with DMSO, 5 mg/kg RARα/β agonist AM80 (Sigma Aldrich), or 1 mg/kg pan-RAR antagonist AGN194310 every other day for a week until euthanasia. To inhibit S1P-signaling pathways, mice were administered FTY720 (Cayman Chemical) diluted in 2% (2-Hydroxypropyl)-β-cyclodextrin (Sigma-Aldrich) or vehicle daily via i.p. injection (1μg/g) for a week until euthanasia. In all experiments assessing SI T_{RM} cell maintenance after AGN194310 treatment, mice were injected i.v. with 50μg of T_{REG}-protector (anti-ARTC2.2) nanobody (Biolegend) 30 min before sacrifice to prevent P2RX7-mediated cell death during tissue-processing.[39]

Mouse tissue processing

Spleen and lymph nodes were processed into a single-cell suspension using metal meshes. Livers were meshed through 70μm cell strainers and pellets were resuspended in 35% isotonic Percoll (GE Healthcare) prior to density gradient centrifugation (500g, 20min). Spleen and liver red blood cells were lysed using 1X RBC lysis buffer (eBioscience). SI was cleared of luminal contents and Peyer's patches were excised. Intestines were longitudinally opened, cut into ~1cm fragments which were incubated at 37°C for min with lateral rotation (230rpm) in 10% Hanks' balanced salt solution/HEPES containing dithioerythritol (0.15mg/mL; Sigma Aldrich). Intra-epithelial lymphocytes were then purified using a 44/70% Percoll gradient centrifugation. Flank skin was shaved and depilated and an area of 1-3cm^2 was excised. Skin was incubated in Dispase II (2.5mg/mL; Roche) for 90min at 37°C. Epidermal and dermal layers were separated, placed in Collagenase III (3mg/mL; Worthington) and DNAse I (5μg/mL; Roche), chopped into fine pieces and further incubated for 30min at 37°C. Digested skin was homogenized into a single-cell suspension and sequentially passed through 70μm and 30μm nylon mesh.

Flow cytometry

Mouse cells were stained at 4°C for 60 min with the following antibodies (all purchased from BD Bioscience, Biolegend or ThermoFisher): anti-B220 (RA3-6B2), anti-CD8α (53-6.7), anti-CD8β (H35-17.2), anti-CD11a (M17/4), anti-CD11b (M1/70), anti-CD18 (M18/2), anti-CD38 (90), anti-CD39 (Y23-1185), anti-CD43 (S11), anti-CD44 (IM7), anti-CD45.1 (A20), anti-CD45.2 (104), anti-CD45RB (16A), anti-CD49a (Ha31/8), anti-CD55 (RIKO-3), anti-CD62L (MEL-14), anti-CD69 (H1.2F3), anti-CD73 (TY/11.8), anti-CD101 (Moushi101), anti-CD103 (2E7), anti-CD122 (5H4), anti-CD127 (A7R34), anti-CD218a (P3TUNYA), anti-CXCR3 (CXCR3-173), anti-CXCR6 (SA051D1), anti-CX3CR1 (SA011F11), anti-Integrinβ7 (FIB27), anti-KLRG1 (2F1), anti-Ly6A/E (D7), anti-Ly6C (HK1.4), anti-MHCII (M5/114.15.2), anti-NK1.1 (PK136), anti-NKG2D (CX5), anti-PD-1 (29F.1A12), anti-TCRβ (H57-597), anti-TCRγδ (GL3), anti-Thy1.1 (OX-7), anti-Thy1.2 (53-2.1), anti-Vα2 (B20.1). For transcription factor staining, cells were fixed and permeabilized using FoxP3 Transcription Factor staining buffer set and stained with the following antibodies (all purchased from BD, Biolegend, Cell Signaling or ThermoFisher): anti-Bcl2 (3F11), anti-Bim (C34C5), anti-Eomes (Dan11mag), anti-FoxP3 (FJK-16s), anti-GATA3 (L50-823), anti-Ki67 (SolA15), anti-RORγt (Q31-378), anti-Runx3 (R3-5G4), anti-Tbet (4B10) and anti-TCF1 (C63D9). Human cells were stained at 4°C for 60 min with the following antibodies (all purchased from BD Bioscience, Biolegend or ThermoFisher): anti-CD8α (HIT8a), anti-CD69 (FN50), anti-CD103 (Ber-ACT8). Dead cells were excluded from analysis using DAPI (0.5μM; Biolegend), eFluor506, Zombie Yellow or Zombie NIR fixable live/dead (Biolegend). For flow cytometry experiments, samples were acquired on a 5-laser BD Fortessa X20 or 5-laser Cytek Aurora. For cell sorting experiments, CD8$^+$ T cells were enriched using a 5-laser BD FACSAria III (BD Bioscience) or a 4-laser Beckman Coulter Cytoflex SRT (>95% purity). Data was analysed on Flowjo v10 (Treestar) or OMIQ (https://www.omiq.ai/).

T cell stimulations and cytokine staining

For the assessment of cytokine production *in vitro*, single cell suspensions of processed tissues were cultured in complete RPMI in the presence of GP_{33-41} (KAVYNFATM) or $OVA_{257-264}$ (SIINFEKL) peptide, brefeldin A (10 μg/mL; Sigma-Aldrich), and P2RX7 inhibitor A-438079 (10 μM, Santa Cruz Biotechnology) for 4h at 37°C. For intracellular staining, cells were processed using BD fixation and permeabilization kit and stained with the following antibodies (all purchased from BD, Biolegend, or ThermoFisher): GranzymeA (GzA-3G8.5), Granzyme B (QA16A02), IL-2 (JES6-5H4), IFNγ (XMG1.2) and TNFα (MP6-XT22).

Flow cytometry high dimensional analyses

Flow cytometry data was scaled using hyperbolic arcsine (asinh) transformation with OMIQ cloud platform (https://www.omiq.ai/). UMAP dimensionality reduction was performed with OMIQ. One-SENSE analysis was performed in R as described,[84] with the

exception that UMAP dimensionality reduction was used instead of t-SNE. UMAP and one-SENSE plots were color coded in R using the *ggplot2* package. Heatmaps and correlation plots were generated using asinh transformed median expression in R using the *pheatmap* R package.

Immunofluorescence and confocal microscopy

SI was collected and fixed in 4% PFA for 4 h, washed in PBS and dehydrated in 30% sucrose (w/v in PBS) before being embedded in OCT freezing medium. Tissue sections of 18 μm thickness were cut using a cryostat (Leica CM3050S) and air-dried before being fixed in ice-cold acetone for 5 min, dried and then blocked for 45 min in PBS containing 2.5% goat serum 2.5% donkey serum at room temperature. Sections were stained with primary antibody overnight at room temperature (anti-Thy1.1-AlexaFluor647, anti-Lyve1-eFluor570, anti-EpCAM-biotin and anti-CollagenIV). Slides were washed in PBS and stained with a Streptavidin-conjugated DyLight 800 and anti-rabbit AlexaFluor 405 for 1 h at RT. Stained sections were mounted in ProLong Diamond antifade reagent and images were acquired on a LSM980 spectral confocal microscope (Zeiss) on a 40× oil (NA 1.4) objective using 405nm, 488nm, 561nm, 639nm and 730nm laser lines via Online Fingerprinting mode. Images were spectrally unmixed through single-color reference spectra, and Z-stacks were scanned at 1024×1024 pixel resolution and a 50% overlap. Post-acquisition processing was performed by applying a Gaussian filter, residual spectral spillover corrected using the Channel Arithmetics XT function and 3D surface rendering were all performed in Imaris 9.3.1.

Retinoic acid quantification

Blood was collected and processed under dark conditions. SPF mice were administered i.p. with 50mg/kg of atRA (Sigma-Aldrich) dissolved in cornoil 90 min before blood collection to serve as positive control. Serum was run on a retinoic acid ELISA kit (MyBiosource, MBS706971) according to manufacturer instructions. Briefly, samples were incubated with 50 ml HRP-conjugated antibody for 40 min at 37°C, washed 5 times with wash buffer, and incubated with TMB substrate for 20 min at 37°C. The reaction was quenched, and absorbance was measured of each well using a micro-plate reader (FLUOstar Omega, BMG Labtech) set to 450 nm with wavelength correction set to 540nm.

CRISPR/Cas9 gene editing of CD8$^+$ T cells

sgRNA targeting *Cd19* (5'-AAUGUCUCAGACCAUAUGGG-3' and 5'-GAGAAGCUGGCUUGGUAUCG-3'), *Hic1* (5'-AGUGUGCGGAAAGCGCGGAG-3' and 5'-CUUGUGCGACGUGAUCAUCG-3'), *Itgae* (5'-GUCAUGGUGGUACUUACUGA-3' and 5'-GAUUGCCUCAGACCCCAAAG-3'), *P2rx7* (5'-UGAGCGAUAAGCUGUACCAG-3' and 5'-UAUCAGCUCCGUGCACACCA-3' or *Tbx21* (5'- UGAACUUGGACCACAACAGG-3' and 5'-GCGGUACCAGAGCGGCAAGU-3'), were purchased from Synthego (CRISPRevolution sgRNA EZ Kit). sgRNA/Cas9 RNP were formed by incubating 1μL of sgRNA (0.3nmol/μL) with 0.6μL Alt-R S.p. Cas9 Nuclease V3 (10mg/mL; Integrated DNA Technologies) for 10min at room temperature. Naïve T cells were resuspended in 20μL P3 buffer (P3 primary cell 4D-Nucleofector X Kit S; Lonza), mixed with sgRNA/Cas9 RNP and electroporated using Lonza 4D-Nucleofector system (pulse code: DN100). Cells were rested for 10 min at 37°C before i.v. transfer. 1×10^5 P14 or OT-I cells edited with control (*sgCd19*) and target guides were mixed at 1:1 ratio and were transferred intravenously. Mice receiving edited naïve T cells were infected with LCMV 4 days following cell transfer.

Retroviral transduction of CD8+ T cells

Retroviruses were produced using Plat-E cells (Cell Biolabs) which were transfected with pCL-Eco, pMSCV-IRES-GFP II (pMIG II) and pMSCV-IRES-Ametrine II (pMIA II) based vectors. Plat-E cells were seeded in 96-mm dishes at a density of 7×10^6 cells 12 hours before transfection with 14mg of pLMPd-Ametrine and 7mg of pCL-Eco plasmid DNA using the CalPhos Mammalian Transfection kit (Takara). Viral supernatants were harvested 48 hours later and filtered (0.45mm; Millipore). A truncated version of human RARα (RARα403)[32] cDNA was cloned into pMIG II vector. Mouse *Ccr9* cDNA was cloned into pMIA II vector. Purified naïve P14 CD8$^+$ T cells were in vitro activated with anti-CD3 (145-2C11) and anti-CD28 (37.51) (5mg/mL for each; both from BioXCell) for 24 hoursand were ''spinfected'' with 0.5mL of retroviral supernatant in 24-well plates coated with Retronectin (32mg/mL; Takara). CD8$^+$ T cells were further expanded for 3 days in the presence of IL-2 (25U/mL; Peprotech). Transduction efficiency was determined by Ametrine or GFP expression. Cells transduced with EV-GFP and CCR9-Amt or EV-Amt and dnRARα-GFP retroviruses, and were mixed at 1:1 ratio. 2×10^5 transduced cells of the relevant specificity were administered intravenously in mice that were infected with LCMV Armstrong or Lm-OVA one day before.

ATAC-seq

WT and *Tbx21*$^{-/-}$ OT-I cells were isolated from the SI 8 d following LCMV-OVA infection. CD69$^+$ OT-I cells were sorted and cryopreserved in DMSO (10%). Frozen cells were thawed and washed once in cold PBS. 70,000-200,000 cells were lysed using the 10x single-cell ATAC lysis buffer and centrifuged for 10 min at 4°C/500g. Transposition reaction was performed using Illumina Tagment DNA TDE1 Enzyme and Buffer Kits (FC-121-1030), using 12.5 μL 2x TD Buffer, 10.5 μL H2O, and 2 μL transposase per reaction, and incubated at 37°C for 30min. TE Buffer was added to halt the transposition reaction, then the product was purified using Qiagen Minelute (28004). The elute underwent PCR using Phusion High-Fidelity PCR MasterMix (NEB, M0531S) as follows; 5 min of initial extension at 72°C, followed by 16 cycles of PCR (98°C/15s, 63°C/30s, 72°C/60s), followed by final extension (72°C/3min). The resulting product was purified using AMPure XP Beads (A63881), eluted in 20 μL H2O, and quantified using a Qubit

dsDNA HS Assay Kit (Invitrogen) and a High Sensitivity DNA chip run on a Bioanalyzer 2100 system. The final product was sequenced on a NovaSeq. For each bulk ATAC-seq library, adapters were trimmed, and fastq reads were aligned using Bowtie2 to the *Mus musculus* reference genome (GRCm39/mm39). PCR duplicates were removed such that only one representative read was selected per unique pair of transposition events. Chromatin accessibility peaks were called using MACS2 using custom parameters for ATAC-seq (nomodel, nolambda, keep-dup, all call-summits), and a signal track in bdg form was emitted from the peak calling function that was subsequently converted into a.bigwig for visualization with the SPMR flag. Across all chromatin accessibility samples, we computed a consensus peak set and counts table using a previously described approach of aggregating peak summits.[85] Motif analyses were conducted using *chromVAR* and *motifmatchR*. For the T-bet directed ChIP-seq data (SRA273724[86]), fastq reads were aligned using Bowtie2 to the *Mus musculus* reference genome (GRCm39/mm39) and were normalized to the library size.

RNA-seq

To profile the transcriptome of effector $CD8^+$ T cells cultured with RA and TGF-β, naive $CD8^+$ T cells were enriched from spleen and lymph node suspension using CD8 EasySep kit (StemCell Technologies) as per manufacturer's protocol. Enriched $CD8^+$ T cells were activated in 96-well plates coated with anti-CD3 and anti-CD28 (1mg/mL) and cultured in complete RPMI (10% FCS, 200mM L-glutamine, 1M HEPES, PenStrep (10000U/mL penicillin + 10000μg/mL streptomycin), 0.5mM β-mercaptoethanol) with IL-2 (10ng/mL), IL-15 (10ng/mL) in the presence or absence of RA (10nM) and TGF-β (10ng/mL). mRNA was isolated after 7 d using the RNeasy Micro kit (Qiagen). Samples were sequenced at Micromon Genomics, Monash University. RNA quality was tested and samples were prepared using the Illumina Truseq stranded mRNA sample preparation kit. Sequencing was then conducted on MGI-2000RS with a PE 100bp cartridge. To profile the transcriptome of dnRARα expressing T_{RM} cells, congenically marked naïve P14 cells were activated and transduced with empty (Ctrl-RV) or dnRARα (dnRARα-RV) retroviruses as shown above. Transduced cells were co-transferred in LCMV-infected mice, and $CD69^+$ T_{RM} cells from the liver and SI were sorted 14 d p.i. To profile the transcriptome of T_{RM} cells following RA signaling blockade, congenically marked naïve P14 cells were transferred into LCMV-infected mice. At >30 d p.i., mice were treated with DMSO or AGN194310 (RA antag.) every other day for 6 d and $CD69^+$ P14 T_{RM} cells were sorted from the liver and SI the following day. For both Ctrl and dnRARα or DMSO and RA antag, T_{RM} cell samples, mRNA was isolated using the RNAeasy Micro kit (Qiagen) and was converted into cDNA using High Capacity cDNA Reverse Transcription Kit (Thermofisher). Libraries were prepared using the SMART-seq HT Plus kit (Takara/Clontech) according to manufacturer's instructions. Sequencing was then conducted at the WEHI Advanced Genomics Hub on an Illumina NextSeq 2000. Data on Effector $CD8^+$ T cell cultures and RA antagonized SI T_{RM} cells were analyzed as follows: raw fastq files were processed using the RNAsik pipeline,[87] sequence reads were mapped to the *Mus musculus* genome (GRCm38/mm10) using *STAR*, and reads mapping to Ensemble annotated genes were counted with *featureCounts*. For the Mackay et al.[13] (GSE70813) data, summarized raw counts were downloaded from GEO, and HSV T_{EM} and T_{CM} cell spleen samples were treated as one group, referred to as T_{CIRC} cells (HSV), and LCMV T_{EM} and T_{CM} cell samples were treated as one group, referred to as T_{CIRC} cells (LCMV). For these data sets, genes without Entrez Gene IDs were filtered, as were genes which failed to achieve a count above 10 in all samples in at least one biological group. The Mackay data was further processed by filtering genes annotated as 'rRNA' and then applying the imputation strategy published previously.[17,88] For these data sets, counts-per-million (CPM) values were calculated, using scaling factors derived from the TMM method,[89] then $\log_2$ transformed with a prior count of 1, followed by application of the normalization method *RUV-III*[90] with biological replicates nominated as replicates, mouse housekeeping genes nominated as 'negative control' genes, and $k = 1$ factors of unwanted variation. Normalization success was assessed with relative log expression plots,[91] PCA plots,[92] and p-value histograms. The *edgeR* package was used to fit gene-wise negative binomial generalized linear models for the experimental design with the output from *RUV-III* as an additional model covariate, where the TMM scaling factors and a prior count of 1 were used. Likelihood ratio tests were employed to test for differential expression (DE), where a gene was judged to be differentially expressed if the Benjamini and Hochberg adjusted p-value was less than 0.05. For the effector $CD8^+$ T cell culture data, interaction was inferred using the standard interaction contrast for a 2x2 factorial design. DE results for SI T_{RM} were obtained by analysing Mackay SI T_{RM} and T_{CIRC} (LCMV) cell samples only, using the steps outlined above. The core T_{RM} cell gene signature was obtained as described previously.[75] logFC ($\log_2$-fold-change) and standardised logFC estimates, i.e. empirical Bayes moderated t-statistics, were calculated by applying *limma* to TMM adjusted logCPM values, fitting gene-wise linear models for the experimental design with the output from *RUV-III* as an additional model covariate, where the 'trend' and 'robust' options were specified. Skin, liver, and SI logFCs were derived from three separate analyses of the Mackay data, applying the steps outlined above to the following samples: (1) skin T_{RM} and T_{CIRC} cells (HSV), (2) liver T_{RM} and T_{CIRC} cells (LCMV); and (3) SI T_{RM} and T_{CIRC} cells (LCMV). Core T_{RM} cell signature logFCs were calculated by averaging the logFC estimates obtained for skin, liver, and SI. For the dnRARα T_{RM} cell data set, files were aligned to GRCm39/mm39 using *STAR*. Reads were mapped to *Ensembl* annotated genes (GRCm39 Ensembl release 105) and counted using *featureCounts*. Counts were loaded into *R* with samples grouped by tissue and genotype status. Genes were filtered using *edgeR* 'filterByExpr' with a 'min.count' of 10 and 'min.total.count' of 15. Normalization factors were calculated with the *edgeR* TMM method. Surrogate variable analysis was used to remove unwanted noise and batch effects, using the *sva* package.[93] Surrogate variables were calculated with the 'svaseq' function using gene counts, a model matrix constructed from the sample groups and a null model. *limma* 'RemoveBatchEffects' was applied to the log count-per-million and surrogate variables with PCA and MDS plots used to evaluate and select a model with 4 surrogate variables. Statistics for association, i.e. log odds ratios (LOR), were calculated by constructing a two-way contingency table counting the number of genes with concordant/discordant logFCs, and p-values for association

were obtained by applying *Fisher's exact test* to the table. Barcode enrichment plots were generated using *limma*, and gene set enrichment p-values were calculated using the function *fry*. Heatmaps were produced from *RUV-III* normalized data, using gene-wise standardization, producing a Z-score, with genes clustered by Pearson correlation. UpSet plots were made with the package *UpSetR*.

16S rRNA-seq

Genomic DNA extraction and 16S rRNA gene amplicon library construction was performed following the Earth Microbiome Project protocols (https://dx.doi.org/10.17504/protocols.io.kqdg3dzzl25z/v2) and sequenced on an Illumina MiSeq. Sequence data processing and microbiome profiling was performed using the *QIIME2* platform (v.2021.4.0). Specifically, quality filtering was performed using default cutoffs, Deblur was used for sub-operational OTU (sOTU) picking after trimming reads to 150bp, and taxonomic classification was performed using the sklearn-based classifier trained on the Greengenes 13_8 16S database. All subsequent analyses were performed in R (v.4.2.3) using the *qiime2R*, *tidyverse*, *vegan*, *phyloseq*, and *ComplexHeatmap* libraries. sOTUs with a mean relative abundance < 0.1% in both mouse genotypes were removed from the dataset before further analysis. Between-sample (beta) diversity was calculated using the Bray-Curtis dissimilarity index on OTU-level data and visualized using Nonmetric Multidimensional Scaling.

QUANTIFICATION AND STATISTICAL ANALYSIS

Statistics analyses were calculated by performing unpaired or paired t-test, One-way ANOVA test with Tukey's post-test using Prism 10 (GraphPad). *$p < 0.05$, **$p < 0.01$, ***$p < 0.001$, and ****$p < 0.0001$.